
**Technical University of Crete**
**School of Electrical and**
**Computer Engineering**

**Diploma Thesis**

# Development of a Hyperspectral Microcamera

Christodoulou Theofilos

**Committee:**

**Professor Balas Costas (Supervisor)**

**Professor Kostas Kalaitzakis**

**Dr Nathanail Kortsalioudakis**

**Chania, March 2018**


**Technical University of Crete**
**School of Electrical and**
**Computer Engineering**

**Diploma Thesis**

# Development of a Hyperspectral Microcamera

Christodoulou Theofilos

**Chania, March 2018**

# “Development of a Hyperspectral Microcamera”


## Abstract

The purpose of this study is to test the feasibility of creating a hyperspectral imaging device, utilising a single rotating dichroic filter as a spectral scanning mechanism. Hyperspectral imaging stands for the acquisition of distinct spatial information from many, typically hundreds, individual spectral components within the electromagnetic spectrum. The examination of the spectral composition of light at each pixel, namely spectral imaging, is able to provide qualitative and quantitative information about the physical and chemical structure of matter, in a non-invasive and non-destructive manner. The proposed system does not compromise spatial resolution, as it uses the entire sensor to capture spatial information at each exposure. A rotating dichroic filter acts as a tunable band-pass optical filter, used to selectively isolate spectral components and, eventually, scan across the electromagnetic spectrum. The ability to tune a dichroic mirror, derives from the nature of the angle of incidence as a determinative factor for its frequency response. In this particular design, a triple-band band-pass dichroic filter is used, along with a color camera, in order to reduce the total number of exposures needed to acquire the desired spectrum. The precise rotation of the filter is achieved using a Stepper motor, that is driven with an Arduino equipped with the Arduino Motor Shield. The proposed method is, ultimately, able to assist spectral imaging with remarkable scalability and optimal reusability of the optical and mechanical components of the device. Further optimization of this system can lead to the construction of a compact, largely accessible, real-time hyperspectral imaging device.

# Table of Contents

# List of Figures

## CHAPTER 1



## CHAPTER 2

## CHAPTER 3



## CHAPTER 4

# Chapter 1:

# Light and Spectral Information

# 1. Light and Spectral Information

## 1.1 Nature of light

The nature of light has long been studied and discussed, especially due to its duality. It is fundamentally considered to act both as a particle, namely photon, and as a wave of electromagnetic energy. Therefore, vast research has been occupied to shed light upon the laws that govern its behavior, as it moves and interacts with other particles.

*[Figure 1.1] Splitter Cubes illuminated by flash light*

Observed as a wave, light primarily consists of many spectral components, each one having its distinctive energy, wavelength and frequency. These characteristics, actually, serve as the fundamental aspects of each spectral component and are, in principle, administrative in regard to the way it interacts with matter. Consequently, it is crucial to be able to identify the spectrum of a beam of light, or -in other words- extract quantitative and qualitative information about the spectral components that contribute to form the perceived beam, as its composition will virtually dictate its behavior across a certain optical path.

### 1.1.1 The Electromagnetic Spectrum

As an electromagnetic wave, light is considered to exist having frequency, wavelength and photon energy levels among the range illustrated by the electromagnetic spectrum, and is classified accordingly.

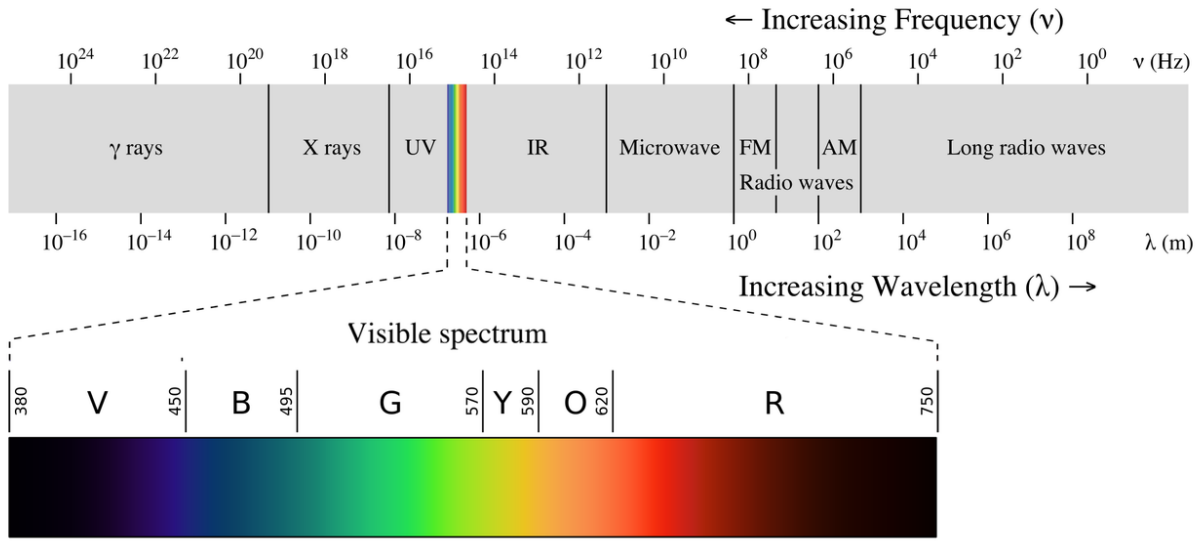


*[Figure 1.2] The Electromagnetic spectrum*

Gamma rays and high energy gamma rays, are considered to have the greatest energy among the entire spectrum, which is calculated to be above 100 keV. They are characterized by short wavelengths, typically less than 10 picometers ($10^{-11}$ m), and frequencies above 10 exahertz ($10^{19}$ Hz). This type of electromagnetic energy is mostly associated with cosmic rays and other astronomical processes. Photons of these energy levels can experience Compton scattering by colliding with charged particles.

X-ray photons have less energy than the gamma ray counterparts, approximately below 100 keV, while above 100 eV, and frequency between 30 petahertz ($3\times10^{16}$ Hz) and 30 exahertz ($3\times10^{19}$ Hz). Their wavelength varies in the range 0.1 nm to 10 nm. X-rays can be fatal to humans after long exposure. They have been largely utilized, though, for instance in health sciences, including medical radiography, due to their ability to penetrate soft tissue like skin, while absorbed by

harder tissue like bones. An illustrative instance is Computed Tomography, a commonly used technique to picture the structure of bones. X-ray photons can, aside absorption, experience Rayleigh scattering, as well as Compton scattering under certain circumstances and are considered as ionizing radiation.

Ultraviolet radiation comes with longer wavelengths, ranging from 10 nm to approximately 400 nm, and frequency between approximately 790 Terahertz ($790\times10^{10}$ Hz) and 30 petahertz ($3\times10^{16}$ Hz). It is considered harmful to humans, as for instance being the main suspect for sunburn and eye damage. On the other hand, ultraviolet radiation excites the production of Vitamin D in the human body, which is essential for life and is also utilized in several beneficial applications, including sterilization of medical tools. Shorter wavelengths of ultraviolet are also considered ionizing radiation.

The only part of the electromagnetic spectrum that the human eye is able to detect, is visible light, thus creating our perception as distinct colors, depending on the spectral composition of the observed ray. Visible light is characterized by wavelengths that lie between approximately 400 nm and 700 nm, corresponding to frequencies in the range 400 to 790 terahertz. It can be captured with sensors including Charged Couple Device (CCD) and Complementary Metal–Oxide–Semiconductor (CMOS).

Infrared Radiation (IR) is characterized by even longer wavelength than visible light, typically between 750 nm to 1 mm with respective frequency from 400 THz down to 300 GHz. This type of radiation is associated with black body radiation, as virtually every object emits light in this particular region, according to its temperature. It can be captured with sensors like microbolometers and other thermal sensors, while shorter wavelengths of infrared can also be captured by CCD or CMOS. There has been an increasing interest over this part of the electromagnetic spectrum during the last years, as higher infrared frequencies, as well as longer visible wavelengths, are able to penetrate human skin for a short distance, thus being significantly illustrative when examined in spectral imaging applications, including health sciences [1].

Microwaves occupy the part of the electromagnetic spectrum between 0.1 cm and 100 cm wavelength, which corresponds to frequencies between 300 MHz and 300 GHz. They are vastly used in applications including radars, wireless networks, such as WiFi and point-to-point communication systems, while they are preferred in several applications in telecommunications

and broadcasting. Microwaves can cause dielectric heating when absorbed, for instance from water, and are thereby, also, utilized as a heating mechanism. Fundamentally, this type of radiation can be detected from antennas.

Radio waves are characterized by the longest wavelengths among the spectrum, ranging from 1 mm to 100 km, and the respective frequency range 3 kHz to 300 GHz. Artificially generated radio waves are largely used in applications including radio and satellite communication, broadcasting and radars.

### 1.1.2 Interaction of light with matter

Light can interact with matter in different ways, according to the underlying conditions. Depending on the nature of matter as well as the intrinsic characteristics of the observed ray, such as frequency, light can fundamentally be absorbed, scattered, reflected or refracted. It is also possible for more than one concurrent electromagnetic waves -or spectral components- to interfere, as long as certain conditions are met.

Scattering

Scattering of light refers to the elastic or inelastic collision of photons with particles of size comparable to the radiation's wavelength. Practically, moving photons are forced to deviate from their trajectory as they collide with particles, mainly due to inherent localized non-uniformities of the material they travel into. Scattering, along with absorption, is responsible for the visible appearance of most objects, including the blue color of the sky during daytime, as well as its red color upon sunset. Two common instances of this process are Rayleigh scattering and Compton scattering, with the first being observed, for instance, as the color of the sky, while the latter is only feasible on high energy photons, such as X-rays.

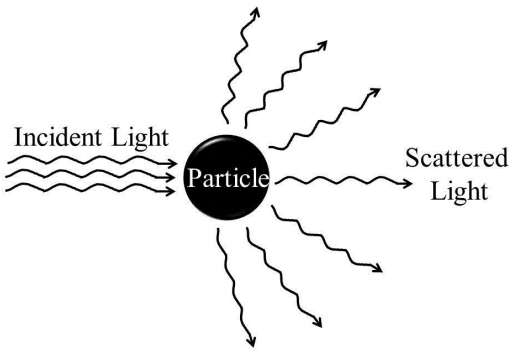


*[Figure 1.3] Scattering of light*

Absorption

Light can also be absorbed by atoms, and particularly their electrons, as a packet -namely quantum- of energy that is transformed and eventually consumed from the receiver. This can be observed on the absorber, for instance, as heat buildup -namely thermal energy- or even electron excitation, depending on the characteristics of the interacting light. In several cases, the energy of an absorbed photon can reveal information about the intrinsic energy levels, or even the identity, of the absorber. Absorption is also responsible for the visible appearance of objects.

Reflection – Refraction

As light moves, it maintains a certain speed, depending on the material it travels into, for instance approximately $3.00\times10^8$ m/s in vacuum. The refractive index (n) describes how the speed and the wavelength of light are affected inside a transmission medium and is calculated as

$$n=\frac{c}{\upsilon} \quad ,$$

where $c$ is the speed of light in vacuum and $\upsilon$ is the phase velocity of light in the medium.

Similarly, the wavelength in that medium can be described by

$$\lambda=\frac{\lambda_0}{n} \quad ,$$

where $\lambda_0$ is the wavelength of the particular electromagnetic wave in vacuum and $n$ corresponds to the refractive index of the transmission medium.

The speed of an electromagnetic wave of a certain frequency ( $f$ ), though, is given by

$$\upsilon=\lambda\cdot f$$

Consequently, the refractive index ($n$) is also a factor of frequency ( $f$ ). Therefore, different frequency components of an electromagnetic wave, may travel in different speed as they move across the same medium.

When an optical path consists of mediums of varying refractive indexes, light can primarily be reflected or refracted, as its velocity changes when it propagates from one medium to another. The Energy and the frequency of photons are not affected by the refractive index and therefore remain constant upon refraction and reflection. Depending on the underlying conditions, such as the refractive indexes of the materials and the frequency of the electromagnetic wave, light can be perfectly reflected, thus the reflective material can be considered as a mirror, or partially transmitted. The transmitted ray is subject to refraction.

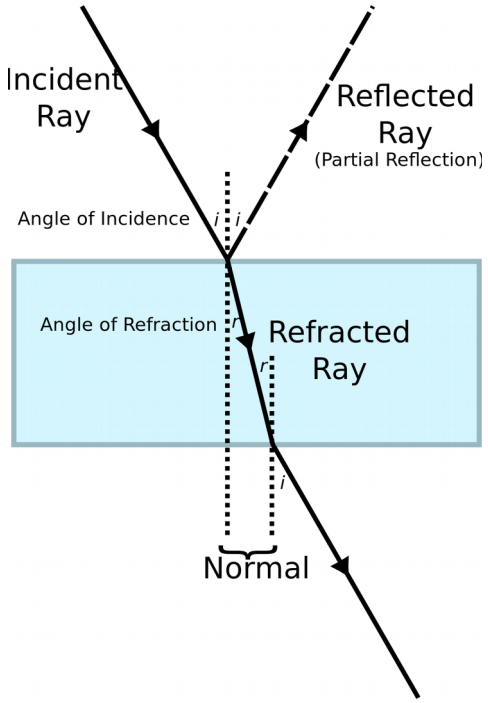


*[Figure 1.4] Reflection and Refraction of light*

According to the law of reflection, the angle of reflection is equal to the angle of incidence on the surface of the medium. In principle, a certain portion of the incident electromagnetic wave is not reflected, but it is rather refracted and transmitted through the medium. Snell's law indicates that, for a given pair of mediums and a wave with a single frequency, the angle of refraction can be calculated as

$$n_1 \sin(\theta_1) = n_2 \sin(\theta_2)$$

where $n_1$ is the refractive index of the first medium and $\theta_1$ the angle of incidence, while $n_2$ corresponds to the refractive index of the second medium and $\theta_2$ to the angle of refraction.

Total Internal Reflection, may also occur in case that the angle of incidence is greater than a critical angle, namely $\theta_{crit}$. Apparently, the refraction angle, as well as $\theta_{crit}$, are dependent upon the refractive index, which is, in respect, a factor of frequency. Therefore, the behavior of an electromagnetic wave as it travels across two given materials with different refractive indexes, is fundamentally dictated by the angle of incidence and its intrinsic frequency.

Multiple unprecedented reflections are referred to as scattering, while the decomposition of light into its spectral components due to the difference in the refractive index they are subject into, is called dispersion.

Interference

As presented in the well-known double slit experiment by Thomas Young in 1801, light cannot defy its nature as a wave and therefore is subject to interference. Interference occurs as two or more waves interact with each other, and practically add together to form a new pattern.

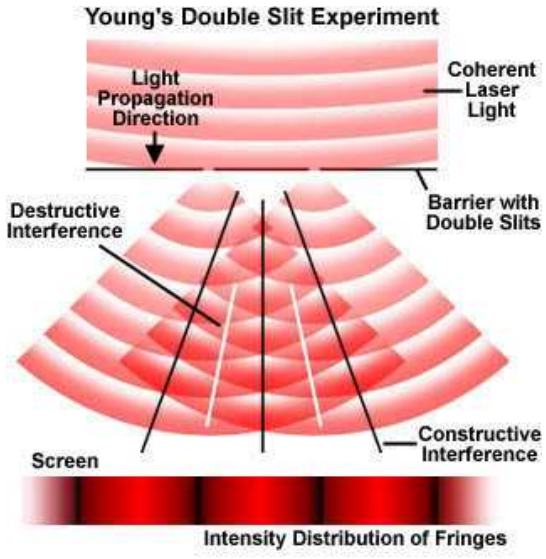


*[Figure 1.5] Double Slit Experiment*

As particular wavelengths interfere, under certain circumstances the interference can be either destructive or constructive. In the double slit experiment, this is illustrated as darker or brighter bands respectively. Constructive interference is observed as the peaks and the troughs of two different wavelengths are perfectly aligned, while destructive interference is the result of peaks of a certain wavelength interacting with the troughs of another.

## 1.2 Spectral Information

The human eye is able to observe light, in three distinct bands within the visible range, as well as its interaction with matter, and consequently lead to several assumptions regarding the physical and structural characteristics of objects. Apparently, the information used to draw the conclusions that compose our perception of the world, is limited by the frequency response of the human eye and therefore some information is hidden, namely invisible. Electromagnetic waves outside the visible region, are, in fact, largely informative too, as each frequency band has its own distinctive characteristics and consequently provides different information about matter. Eventually, almost each spectral component of the electromagnetic spectrum interacts with matter in a different, yet distinctive, way, thus carrying explicit information. The need of obtaining as well as illustrating spectral information has therefore emerged, with honorable advances and applications, shedding light upon the invisible.

By observing the emission, reflection and absorption properties of objects across the spectrum, it is possible to extract information about their molecular and atomic structure, as well as other aspects of their nature. For instance, thermal infrared imaging is utilized as a method to examine objects, based on their radiance in the infrared spectrum, which occurs due to their temperature and is extensively used in surveillance, agriculture, health sciences and other applications [2].

Based on the absorption of infrared light from tissue, infrared spectroscopy reveals information about the chemical structure of molecules [3]. The energy of infrared radiation can selectively cause atomic vibrations when absorbed, while the nature of these vibrations is dictated by the chemical characteristics of molecules, thereby illustrating for instance the structure of bonds. Absorption may also describe the intrinsic energy levels of atoms, providing quantitative and qualitative information, as light is consumed as quanta of energy.

Higher energy electromagnetic waves are also utilized, for instance in Computed Tomography, as they are absorbed by harder and denser tissue in the human body, facilitating the imaging of bones. Visible light, on the other hand, is easily absorbed and scattered by soft tissue like skin, thus making it practically impossible for the human eye to observe what lies beyond.

In fact, each spectral component of light has a different penetration depth according to its wavelength. Penetration depth actually denotes the distance that each distinct wavelength is able

to travel inside a tissue or material, before it is either reflected, or completely scattered and absorbed inside the host body. This implies that imaging, for instance human skin, in different spectral bands, eventually corresponds to imaging in different depths of the tissue [1, 4], which, also, is virtually impossible for the human eye to observe, as it is only able to perceive light as a factor of three fundamental spectral elements: red, green and blue.

Hence, capturing distinct spatial information for each spectral band of interest, namely spectral imaging, can be largely informative, while practically impossible without the development of dedicated tools and techniques.

## 1.3 Spectral Imaging

Spectral imaging is the combination of two well-established scientific methods, optical spectroscopy and imaging. Imaging in multiple distinct spectral bands across the spectrum simultaneously, can provide information formerly unattainable, thus extending the capabilities of imaging far beyond human vision. Spectral imaging systems can be considered multispectral, hyperspectral or even ultraspectral, according to the number of spectral bands they are able to distinguish. Hyperspectral imaging systems can typically obtain hundreds of narrow bands, often within the visible spectrum and beyond. Thanks to Spectral Imaging, scientists are now able to see under the skin [5] or even far into space [6-7].

Still, acquiring and handling this vast amount of information raises numerous new challenges. These challenges include from shortening the long time needed, both for image acquisition and post-processing, to even compressing this information to a level that it can be adequately stored, without compromising resolution. Optimizing a spectral imaging system would result in many trade-offs, including time, storage space, spectral and spatial resolution, cost, even physical characteristics like size and weight. Consequently, several methods of spectral imaging have been proposed, each one having its characteristic advantages and disadvantages.

### 1.3.1 Principles of Spectral Imaging

Spectral imaging stands for the acquisition of spatial as well as spectral information from anything inside the Field of View of an imaging system. This information can be visualized in the form of a three-dimensional dataset I(x, y, λ), namely the Spectral Cube, where each Two-

Dimensional (2-D) image I(x, y) is a factor of light wavelength (λ). Apparently, the third dimension of the spectral cube represents wavelength, so practically it is possible to examine the amount of light detected in the scene corresponding to any particular spectral component of interest, or a narrow spectral band around it. In other words, spectral imaging is capable of providing spectral information for each individual pixel within the acquired image.

Fundamentally, spectral imaging combines two well-established fields: imaging and optical spectroscopy. This is where this scientific method's spatial and spectral analysis capabilities derive from, respectively. The combination of imaging and optical spectroscopy though, is not trivial, as spectral imaging inherits both their intrinsic properties and limitations. In spite of thoroughly understanding these capabilities and limitations, a brief examination of the nature of both imaging and spectroscopy is needed.

Imaging

Imaging is the commonly used science and technology of representing an object's form and properties, by obtaining spatial and temporal information deriving from the way light interacts with it. Imaging practically lies on detecting and visualizing electromagnetic energy, and the interaction of it with matter. Imaging focuses on capturing spatial information about the observed scene, while the distinct spectral information it can obtain are limited, for instance only in three large bands, namely Red Green and Blue, when capturing visible light with a conventional camera. Across the electromagnetic spectrum, there are many bands of interest, from gamma-rays to radio waves, where imaging is utilized as a tool to gather important information about the structural and physical characteristics of objects. As light's interaction with matter is primarily frequency dependent, imaging systems and sensors are mostly optimized to sufficiently detect energy only in one portion of the electromagnetic spectrum, for instance the visible, or infrared.

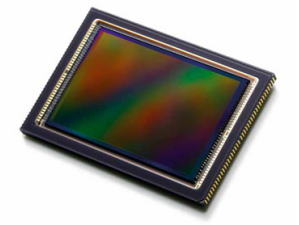

*[Figure 1.6] CMOS Sensor*

As for today, imaging is used by scientists in numerous applications including life sciences, astronomy, physics, chemistry and biology, in order to obtain information about objects based on

their optical characteristics. The most commonly used method is digital imaging, where visible light is recorded with a digital camera, using a Charged Couple Device (CCD) or a Complementary Metal–Oxide–Semiconductor (CMOS). CCD and CMOS sensors, fundamentally, can only measure the amount of light they sense, without any color information. Therefore, they are usually covered with certain optical filters, in order to illustrate the frequency response of the human eye.

## Optical Spectroscopy

Optical Spectroscopy is the science of obtaining and examining the spectral characteristics of matter. Spectral characteristics actually denote the way distinct wavelengths of light interact with a particular medium or object. This kind of information is described by the spectrum, which is the representation of the intensity of each spectral component, or wavelength, of light measured after the interaction. Spectroscopy is in principle indifferent to spatial information.

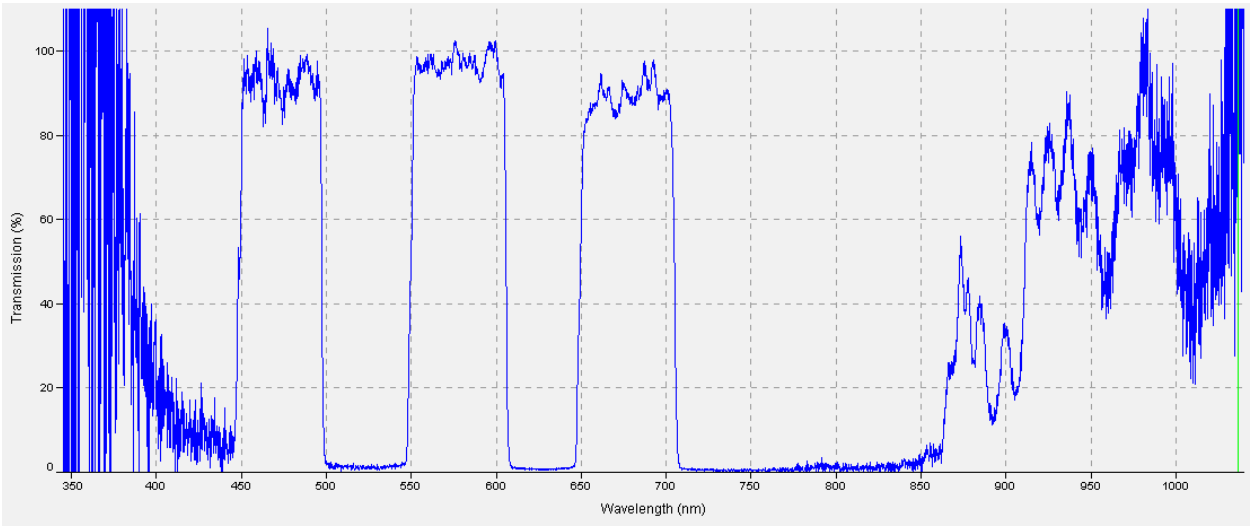


*[Figure 1.7] The Spectrum. Spectrometer measurement illustrated in the form of Spectrum. The horizontal axis represents different wavelengths, while the vertical axis corresponds to the transmission ratio.*

In order to acquire a spectrum, light is dispersed into its distinct spectral components, usually achieved by a prism inside a spectrometer, and then the intensity of each component is measured. The number of distinct wavelengths that a spectrometer can measure denotes the system's spectral resolution.

Using Optical Spectroscopy, it is possible to identify the presence and measure the population of atoms and molecules by observing their spectral signature, namely the distinctive spectrum which derives from their intrinsic energy levels, therefore revealing structural information in a non-invasive and non-destructive manner. Infrared spectroscopy (or vibrational spectroscopy) and Raman spectroscopy, for instance, take advantage of this characteristic and, mainly based on the absorption of infrared radiation from matter, are able to extract information about the structural components of objects **[8-9]**.

Optical Spectroscopy, utilized in various scientific fields, studies the interaction of light with matter, including absorption, emission, fluorescence, reflection and scattering, while focusing in one portion of the electromagnetic spectrum. According to the spectral range of observation, spectroscopy can be classified as microwave, terahertz, infrared, near infrared, visible and ultraviolet, x-ray and gamma spectroscopy.

Spectral imaging systems, apparently, are mainly characterized by their ability to obtain convenient spectral and spatial information, namely their spectral and spatial resolution. Spectral resolution, as in spectrometers, denotes the system's ability to adequately distinguish information between distinct wavelengths, ultimately its capability to resolve spectral features and bands into their separate components. Spatial resolution, on the other hand, describes the minimum distance between two independently measured values or objects in the Field of View (FOV) that can be distinguished by an imaging system.

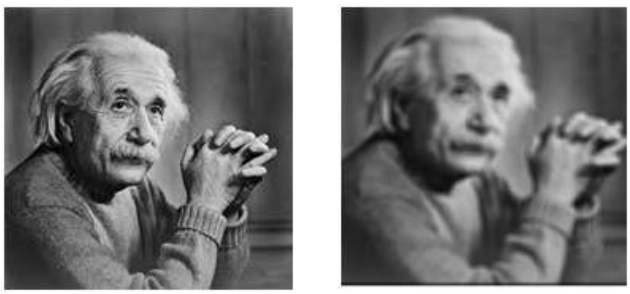

*[Figure 1.8] Spatial Resolution. Image with good (left) and bad (right) spatial resolution*

Spectral resolution mainly derives from the characteristics of the dispersive optics, as well as the spectral response of the sensor or sensors, that the system consists of. Spatial resolution, on the other hand, is primarily dependent upon the optical characteristics of the system, including the Numerical Aperture (NA) of the objective lens, the pixel size of the detector and the

magnification, besides the wavelength of the electromagnetic waves and the signal quality or lighting conditions within the observed scene.

Spectral imaging is widely utilized across many scientific fields, including life sciences, in order to provide information in a non-destructive and non-invasive way. It has proven to be able to assist image-guided surgery [10], as well as the diagnosis of various diseases like gastric carcinomas [11], breast cancer [12], and several skin diseases, including melanoma, acne and psoriasis [13-19]. Other application fields involve ocean research [20], food safety [21] and geology [22]. Also, multispectral and hyperspectral imaging have been suggested as methods for the non-destructive identification of pigments in artworks [23-27].

### 1.3.2 Spectral Imaging methods

Spectral Imaging requires the acquisition of multiple images of the examined object or scene, each one corresponding to a particular wavelength or narrow spectral band. Capturing multiple images, though, requires a long total acquisition time, which stands in contrast to the requirements of many applications, where time constraints are ultimately strict, like in many bio-medical applications. Long acquisition time can also exploit motion artifacts, thus reduce the quality and disguise information of the image captured. Therefore, compromises have to be made in order to achieve high quality spectral imaging, in a limited amount of time.

This challenge has led to the development of various spectral imaging methods, which can be mainly classified as:

- Wavelength-scan methods, that capture the whole image under a particular wavelength at each exposure,
- Spatial-scan methods, that obtain all the spectral information, only from a portion of the image at each exposure, for instance line by line or even pixel by pixel, and
- Time-scan methods, where each obtained image is a superposition of spectral or spatial image information and the actual spectral image is reconstructed through data processing, for example using Fourier transform, at the end of the acquisition.

Some methods for acquiring the whole spectral image at once have also been proposed, but ultimately compromise spectral resolution, spatial resolution, or Field of View (FOV).

Wavelength-scan

Wavelength scan methods perform a full image scan for each distinct observable wavelength. This is primarily achieved with the use of optical filters that restrict particular wavelengths, while transmitting one or more narrow spectral bands. Although this is an efficient method when the filters and the corresponding sensors are carefully selected, it is only applicable when a small amount of distinct wavelengths are required. Therefore, a very common approach is to use varying filters in order to achieve better spectral resolution, using less components, thus reducing size and cost in most cases.

An illustrative instance is the filter wheel [28-30], where a series of optical filters construct a wheel, attached to a motor. As the motor turns, the filters sequentially intersect the optical path, in front of the sensor. The camera has to be properly aligned, as well as synchronized with the wheel, so that each exposure corresponds to a certain filter. The spectral cube, which encompasses the information of the spectral image, can be constructed by stacking the acquired images, each one of which corresponds to a distinct spectral band.

*[Figure 1.8] Filter Wheel. Thorlabs FW1ADF-Filter Wheel with six 1" diameter Dichroic Color Filters*

Instead of using many optical filters, wavelength-scan methods can also be performed using a tunable filter [31-32]. This approach involves Liquid Crystal Tunable Filters (LCTF) [33-34] and Acousto-Optical Tunable Filters (AOTF) [35-36], two commonly used electro-optical components, while eliminating moving parts. The most common LCTF imaging system (Lyot design) [37] consists of a polarizable liquid crystal mounted between two linear polarizers, and acts like a narrow band pass optical filter, the spectral response of which can be selectively manipulated by voltage applied to it.

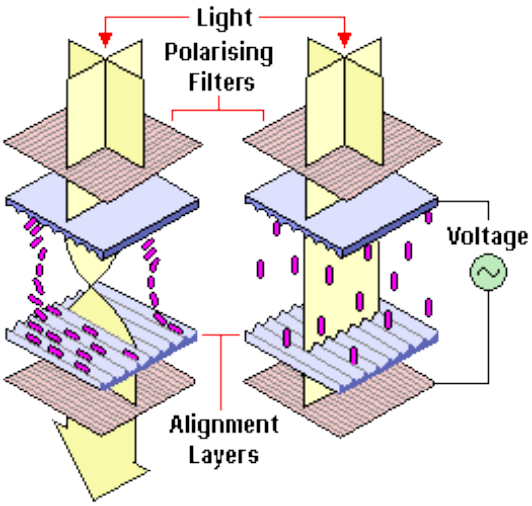


*[Figure 1.9] Liquid Crystal Tunable Filter*

An Acousto-Optical Tunable Filter (AOTF) on the other hand, consists of a crystal, for instance Tellurium dioxide ($TeO_2$), the spectral response of which can be manipulated by sound waves. When applied, these waves are able to deform the crystal, as it practically oscillates with the sound. This can be illustrated as moving periodic planes of compression and expansion of the crystal, which result in a varying refractive index among its body.

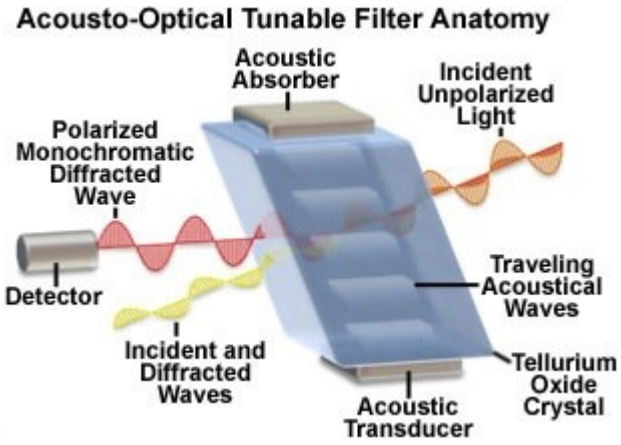


*[Figure 1.10] Acousto-Optical Tunable Filter Anatomy*

The tunable filters presented (LCTF and AOTF) have proven to be very efficient in various spectral imaging applications. They are able to assist a full image scan under particular narrow spectral bands selectively, while their transition is significantly faster compared with the

transition of the filter wheel approach. Yet, the presence of multiple polarizing elements embodied in Liquid Crystal and Acousto-Optical tunable filters, induces significantly low peak transmission values, which could emerge as a limiting factor in several applications.

Spatial-scan

Spatial scan methods, on the other hand, hinge on acquiring the full spectrum of a particular part of the target at each exposure. The image is sequentially scanned, for example line by line or pixel by pixel. The scene is beam-split into the desired wavelength components by using a prism, grating or a patterned filter array and each distinct spectral band is detected by a separate sensor. Apparently, a dedicated scanning mechanism is needed if it is not an intrinsic part of the optical system.

A common approach is multispectral filter-array based sensors, which selectively collect multiple wavelength spectra from a single detector array **[38-42]**.

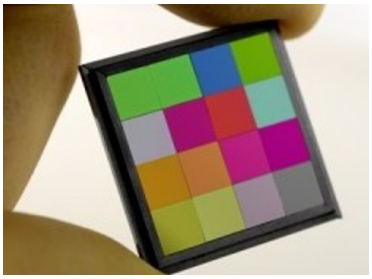

*[Figure 1.11] Multispectral filter-array*

Although spatial-scan methods provide high spectral resolution, they compromise spatial resolution and therefore multiple exposures are required, in order to collect the entire spectral image with sufficient spatial information. The indicated methods are consequently prone to motion artifacts, as they rely upon multiple image acquisitions to obtain the spectral cube, though they have proven to be very efficient in applications where the target is moving linearly.

Time-scan

Time scan methods of spectral imaging do not rely on directly obtaining spectral or spatial information. They in principle acquire a superposition of spatial and spectral information and therefore the acquired data has to be transformed, for instance by performing Fourier Transform, in order to deduce the spectral image.

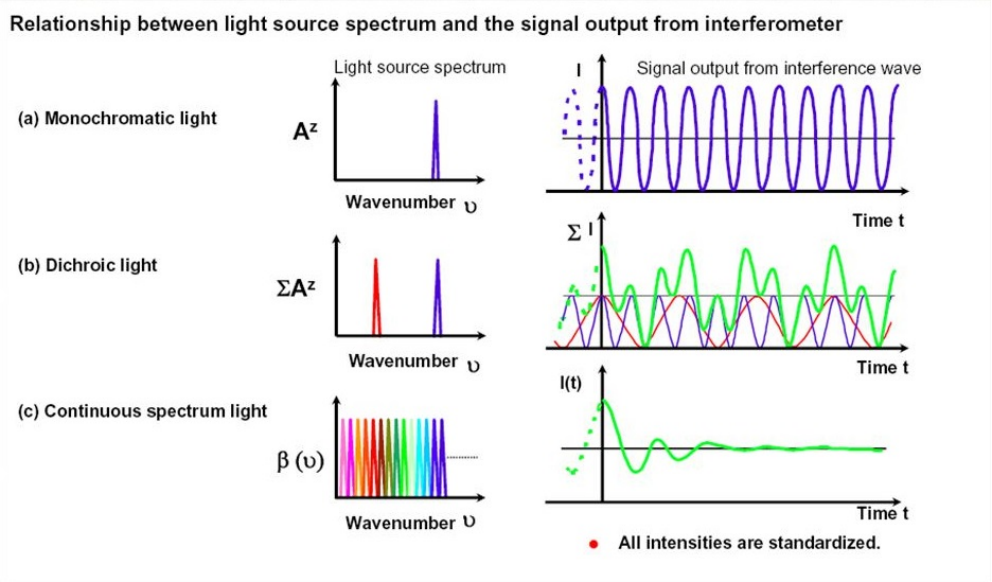


*[Figure 1.12] Relationship between light source spectrum and signal output from interferometer*

Fourier spectroscopy, an illustrative instance of time-scan spectral imaging, exploits the interference nature of light in order to obtain information. The incident beam is split in two parts, each one of which follows a different optical path towards the detector, where the two beams finally meet and interfere with each other.

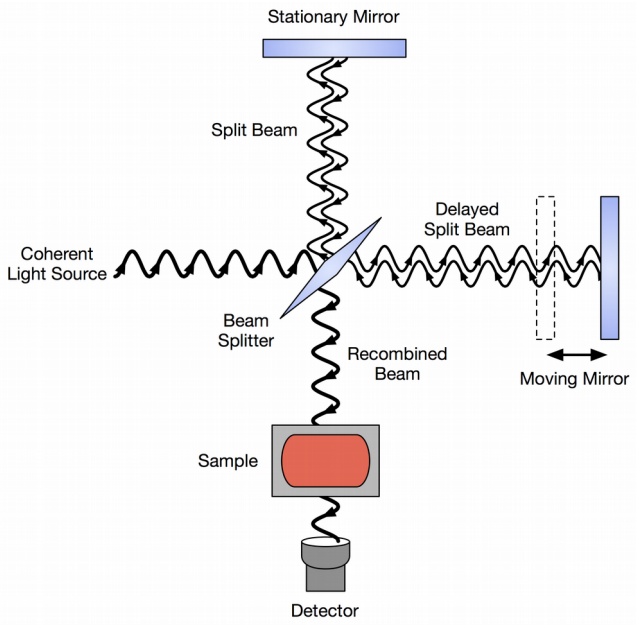


*[Figure 1.13] Schematic diagram of a Michelson interferometer, configured for Fourier-Transform Infrared Spectroscopy (FTIR)*

In pursuance of interference, the two beams have to be out of phase when joint back together, which is achieved by selectively delaying one in contrast to the other. The desired delay is induced by the difference of the distance each ray has to travel before they reconnect. This length difference between the optical paths is called Optical Path Difference (OPD). The intensity of the detected light can be measured as a function of more than one OPDs, where different wavelengths interfere with each other, either constructively or destructively, thus creating the interferogram. The interferogram illustrates the interference characteristics of the detected light and is actually composed of a superposition of spectral and spatial information about the target. It is apparently unique for any distinct image, hence it is feasible to extract the entire spectrum of the observed image, by performing Fourier transform on the acquired data.

This method is characterized by its ability to obtain both spectral and spatial information simultaneously, while each spectral component is constantly measured throughout the acquisition process. This, though, could also be an undesirable aspect in several applications, where only a small amount of spectral bands are required, but still the entire spectrum has to be acquired without regard to the desired spectral range.

All of the spectral imaging methods mentioned, have largely matured throughout the recent years. Despite the substantial advances, though, several defects including cost, and acquisition time, over sufficient spatial and spectral information, have yet to be resolved.

### 1.3.3 The Spectral Cube

The spectral and spatial information captured by a spectral imaging system, can be illustrated in a 3-dimensional dataset, the Spectral Cube. Each pixel of a 2-dimensional image I(x, y) has its own spectrum I(λ). Therefore, each value of the dataset can be accessed as I(x, y, λ) and represents the intensity of a given wavelength (λ) at the pixel (x, y) of the image.

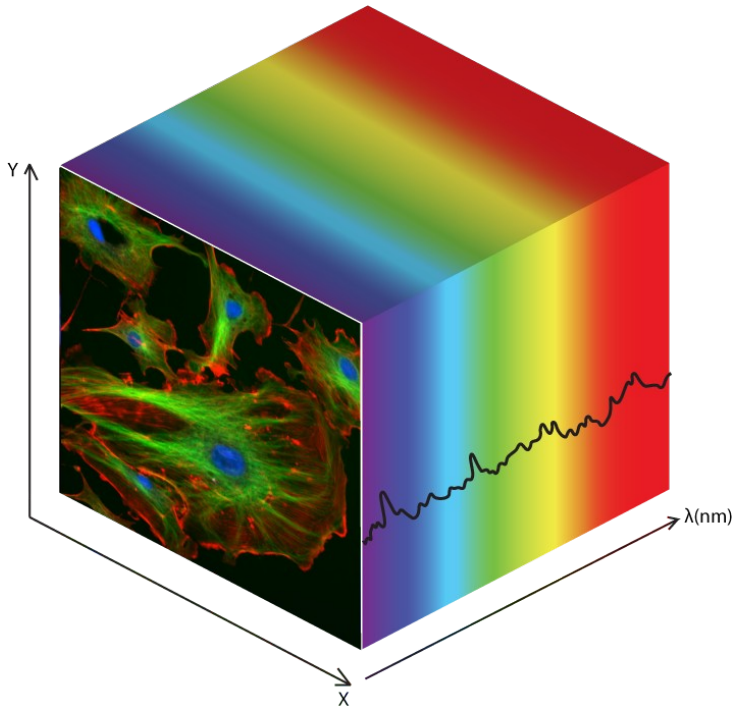


*[Figure 1.14] Schematic representation of a hyperspectral data cube.*

The horizontal and vertical axes x and y correspond to the 2 dimensions of the observed images, while the third axis z represents light wavelength.

One has to consider the spectral cube as a set of gray-scale 2-dimensional images of the same scene, each one corresponding to a particular wavelength, or color. These images actually illustrate the spatial information that derive for the scene, according to the intensity of light of each corresponding wavelength across the image.

Apparently, the number of pixels (x, y) that each gray-scale 2-D image consists of, as well as the ability to explicitly describe spatial information within them, depict the spatial resolution of a

spectral imaging system. Its spectral resolution, on the other hand, is illustrated by the quantity of distinct spectral bands represented across the spectral dimension of the cube I(λ), as well as its ability to provide coherent information about each corresponding spectral component.

In order to construct a spectral cube that embodies legitimate information, compensation has to be made in several cases, in the form of processing the acquired data, depending on the characteristics of the spectral imaging system. For instance, linear unmixing has to be applied in cases where the spectral channels are subject to cross-talk and therefore by nature provide incoherent native spectral information [43]. Other algorithms include demosaicking [44], and various artifact compensating methods [45].

Compression of the spectral cube is also a non-trivial challenge, especially in applications where multiple large spectral cubes are manipulated, as it can greatly reduce the space required to store this vast amount of information, although, with a significant cost in processing time. Consequently, several methods have been proposed in the shake of optimizing the compression ratio as well as the time needed to compress the spectral cube, while maintaining the implicit information intact [46-47].

## 1.4 Statement of Purpose

As presented, spectral imaging has been largely utilized in several scientific fields, including life sciences, as it can potentially provide information of great importance, in a non-invasive and non-destructive manner. As the interest over spectral imaging applications increases, it is essential to create a dedicated system, broadly accessible in terms of size, cost and acquisition time. This study examines the feasibility of creating a spectral imaging system, utilizing a single dichroic filter attached to a motor as a tunable filter.

The proposed system is able to obtain spectral images using the wavelength scan method. A camera equipped with a CMOS sensor captures spatial information, while an optical filter is responsible for filtering the spectral components of incident light, thus selectively feeding the camera with wavelength-specific spatial information. Being able to tune the frequency response of the filter at each exposure, it is ultimately possible to obtain information in more than three distinct spectral bands, in contrast to a conventional camera.

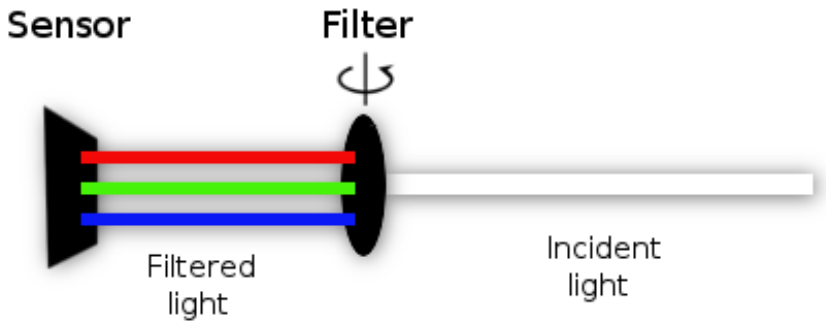


*[Figure 1.15] Wavelength-specific information to Camera Sensor using an Optical Filter*

The ability to tune a dichroic mirror, derives from the nature of the angle of incidence as a determinative factor for its frequency response. By selectively tilting the filter, light that reaches the camera sensor is incident on the filter at a non-normal angle. This deviation from normal incidence alters its frequency response, as different wavelengths are rejected. In fact, its spectral features, like transmission and rejection bands, eventually shift towards shorter wavelengths, depending on the deviation from the normal angle of incidence and the characteristics of the filter.

This study ultimately investigates the sustainability of a rotating dichroic mirror as a tunable filter. This approach can greatly reduce the size and cost, compared with the filter wheel approach, while still utilizing the beneficial aspects of dichroic filters. It is therefore possible to create a small, compact spectral scanning mechanism, able to facilitate any spectral imaging system. Potentially, this kind of tunable filter can be mounted on any conventional camera, including smartphone cameras, constructing a robust spectral imaging system, that could even be used for self-examination.

# Chapter 2:

# Optical Filters – Theoretical Background

# 2. Optical Filters – Theoretical Background

## 2.1 Production and Classification of Optical Filters

Optical Filters, usually a piece of flat glass or plastic, are devices that transmit particular wavelengths of light. They are used to restrict certain wavelengths, while allowing the band -or bands- of interest to pass through. This is achieved by absorbing or reflecting the unwanted spectral part of incident light. According to the way optical filters block light, they are defined as absorptive or dichroic.

An optical filter can be comprehensively described by its frequency response, which illustrates the effect it has on the magnitude and phase of each spectral component of the incident light. According to the frequency response, an optical filter can be mainly classified as longpass, shortpass or bandpass.

### 2.1.1 Absorptive , Dichroic Filters

Optical filters can selectively filter out wavelengths either by absorbing them or by reflecting them, thus rejecting the unwanted portion of incident light. Depending on the nature of wavelength rejection, the filters inherit several distinct characteristics and are, therefore, separated in two main categories, absorptive and dichroic filters.

Absorptive Filters

Absorptive Filters consist of a piece of glass or plastic, infused with various organic or inorganic compounds that absorb certain wavelengths, while transmitting the others. The filter's frequency response derives from the absorption properties of the glass substrate.

This type of optical filter is preferred in applications where noise from unwanted light can be an issue, since they don't reflect any of the incident light, but they rather absorb it. Absorbing light though, can also increase the temperature of the filter, and this characteristic is narrowing the spectrum of applications that filters of this type can be used.

Another discriminating characteristic of the absorptive filters, is their high tolerance on the angle of incidence. Light can be incident on the filter from a wide range of angles and the filter will still maintain its transmission and absorption properties.

Dichroic Filters

Dichroic filters (also called “reflective” or “interference” or “thin film” filters or “dichroic mirrors”) are produced by covering and infusing a glass substrate with a series of optical coatings. Their filtering principal is mainly based on reflecting unwanted wavelengths, while transmitting residual light.

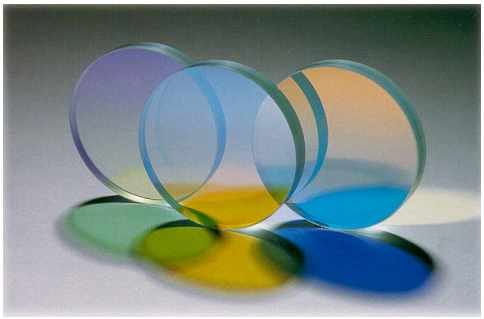

*[Figure 2.1] Dichroic Filters*

Reflective filters can be very accurate, in terms of tuning, upon production, the central wavelength and the width of a spectral band that is going to be transmitted through the filter. This unique capability derives from thin-film interference that is taking place inside the filter. Typically, layers of materials of varying indexes of refraction are added into a dichroic mirror through vacuum deposition, to exploit the interference nature of light waves. Wavelengths selectively interfere with each other, either constructively or destructively, after reflecting and refracting through different thin films of material inside the glass substrate. This results in a very precise spectral response, as long as incident light is perpendicular to the glass substrate, or on a narrow angle of incidence.

By reflecting -rather than absorbing- the unwanted portion of light, dichroic filters do not absorb any unwanted energy, this way avoiding overheating during operation. In some applications, reflection can also be a desirable effect, as incident light can be separated by wavelength into two different sensors or optical paths. Reflection, though, is highly dependent on the angle of

incidence. Tilting a reflective filter will result in a different frequency response, as different wavelengths will interfere, reflect, or be transmitted through the filter.

Dichroic mirrors are particularly suited for applications that demand very high filtering precision, since their exact spectral response can be specifically tuned during production to meet the desired requirements.

### 2.1.2 Longpass, Shortpass, Bandpass Filters

Optical Filters selectively transmit light in a particular range of wavelengths, while rejecting the remainder either by absorbing or by reflecting it and canceling it out. They can usually pass long wavelengths only (longpass), short wavelengths only (shortpass), or one or more bands (bandpass), rejecting both longer and shorter wavelengths around the pass-band. The transition between maximum and minimum transmission can be sharp or gradual and the pass-band can be narrow or wide.

Longpass

Longpass filters are designed to transmit longer wavelengths than the cut-on wavelength of the filter, while rejecting shorter wavelengths.

They can have a very sharp slope (referred to as Longpass Edge Filters) and are described by the cut-on wavelength, where transmission reaches 50% of the peak transmission.

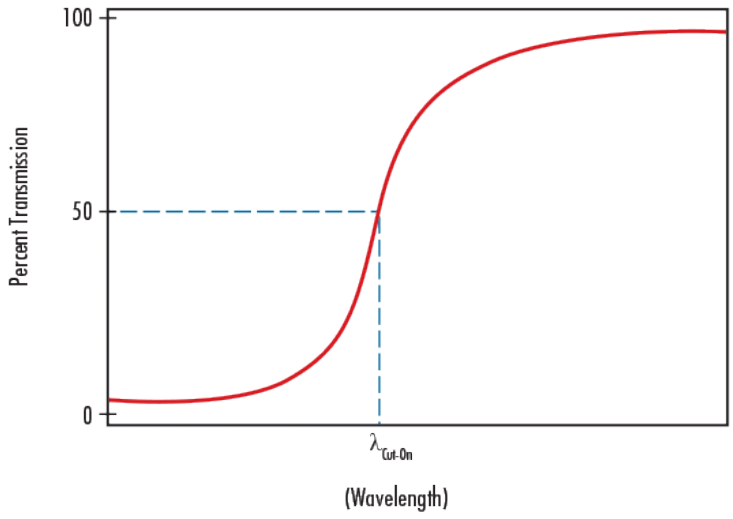


*[Figure 2.2] Illustration of the spectral response of a Longpass Optical Filter*

There are many applications where Longpass filters are used to isolate portions of the spectrum, including industrial or life sciences applications like fluorescence instrumentation and microscopy.

Longpass filters can be utilized in dichroic mirrors and construct a “cold mirror”, reflecting back light only, while transmitting infrared wavelengths.

Shortpass

Shortpass filters attenuate wavelengths longer than the cut-off wavelength, while transmitting shorter wavelengths. They are described by the cut-off wavelength, which denotes the wavelength at which the transmission decreases to 50% of the peak transmission. Shortpass Edge filters derive from shortpass filters with a very steep slope on their spectral response.

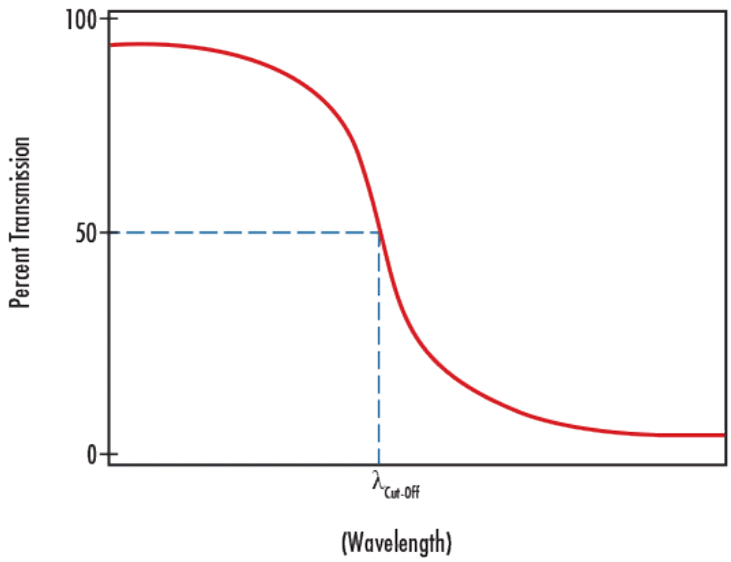


*[Figure 2.3] Illustration of the spectral response of a Shortpass Optical Filter*

Shortpass Filters are useful in various life science applications, including microscopy and fluorescent instrumentation. They are often used as “hot mirrors”, that transmit visible light while reflecting infrared, thus preventing heat buildup that emerges from infrared radiation.

Bandpass

Bandpass filters can be produced by combining longpass and shortpass filters. In Bandpass filters one or more spectral bands are selectively transmitted, while the residual light is rejected. Each pass-band is characterized by its Central Wavelength and Bandwidth, that is calculated according to the Full Width at Half Maximum (FWHM).

A pass-band can be narrow or wide and the transition from minimum to peak transmission can be sharp or gradual. The width of a pass-band can vary from less than an Ångström, or 0.1 nm, to a few hundred nanometers.

Optical Bandpass Filters are ideal for a wide spectrum of applications, including fluorescence microscopy, spectroscopy, clinical chemistry, imaging and astronomy.

## 2.2 Dichroic Band Pass Filters

### 2.2.1 Filtering Principle

Dichroic Filters fundamentally use the principle of reflection in order to selectively transmit or reject wavelengths. By exploiting the interference nature of light waves, though, they are able to achieve very sharp transitions between minimum and maximum transmission. This feature makes them suitable for applications where bandpass optical filters with a very specific frequency response are needed, especially in cases where more than one pass-bands are required.

To construct a dichroic filter, multiple “thin-films” of materials of varying refractive indexes have to be added to a glass substrate, in order to create an optical path which consists of a sequential series of reflective cavities that resonate with the desired wavelengths. By adjusting the width of each “thin-film” and choosing the right indexes of refraction, it is possible to create phase-shifted reflections of each individual wavelength, that interfere with each other. In spite of interference, each layer of material has a width comparable to the wavelength or wavelengths that it resonates with and a different refractive index from the adjacent layers. According to the phase shift induced, the interference can selectively be either constructive or destructive, for each individual spectral component. This way, a pass-band can be precisely tuned, in terms of width

and central wavelength, while the potential of having multiple pass-bands in a single filter arises, as it is possible to create more than one transmission bands, without overlapping..

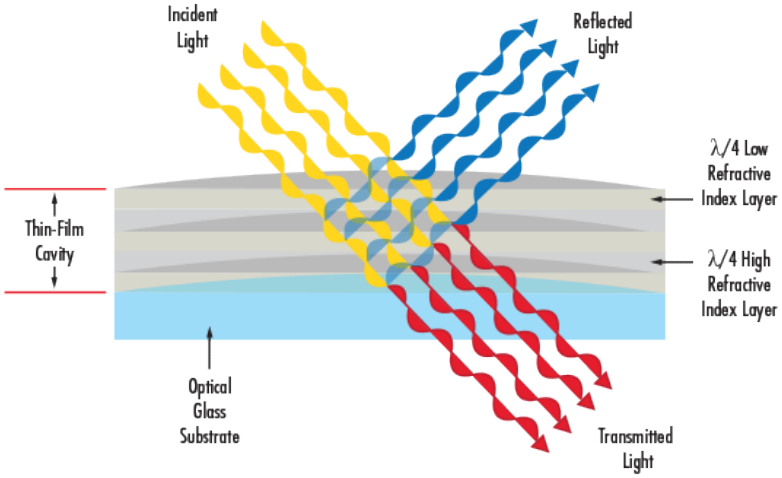


*[Figure 2.4] Deposition of Multiple Layers of alternating High and Low Index Materials onto a Glass Substrate*

In general, the frequency response of a band-pass dichroic filter contains one or more pass-bands. Each pass-band is characterized by its Width and Central Wavelength. The width of a pass-band corresponds to the FWHM (Full width at half of maximum transmission), namely the bandwidth at 50% of peak transmission. The central wavelength is the arithmetic mean of the wavelengths at 50% of peak transmission.

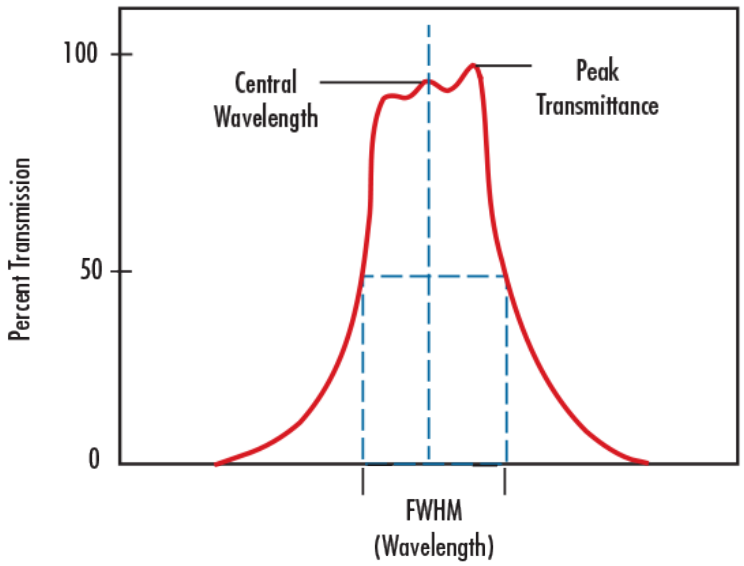


*[Figure 2.5] Illustration of the spectral response of a Band Pass Filter*

Since reflection is the fundamental principle that dichroic filters utilize to achieve the desired transmission and rejection properties, the angle of incidence of light is apparently a determinant in their frequency response.

### 2.2.2 Angle of incidence

The Angle Of Incidence (AOI) describes the angle between the optical axis of the incident light and the axis normal to the surface of the filter, namely 0 degrees. Most dichroic filters are designed to be used at the normal angle of incidence, as a non-normal angle will alter their frequency response, as well as cause polarization. It is important, though, to understand the nature of the angle sensitivity that describes this type of filters.

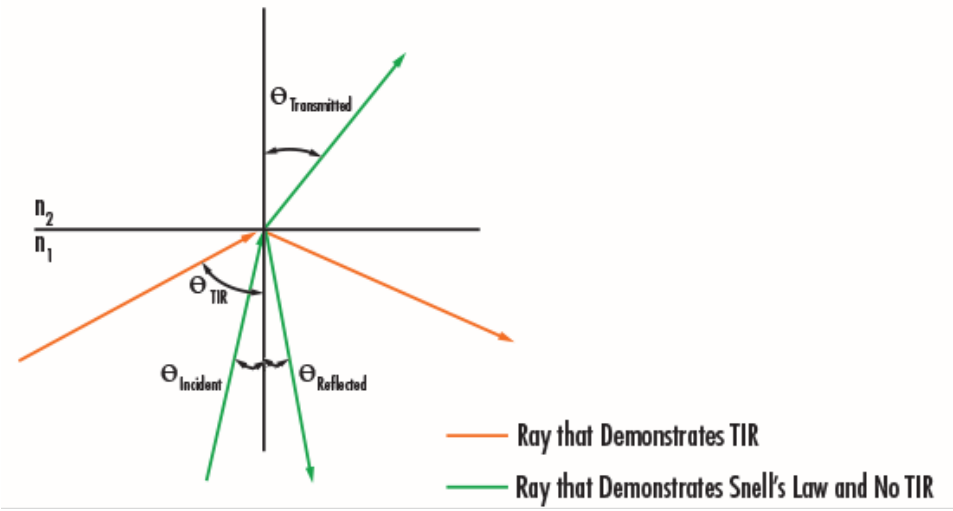


*[Figure 2.5] Reflection, Refraction, Total Internal Reflection (TIR). Light traveling in medium with refractive index $n_1$ meets the surface of another medium with a larger refractive index $n_2$. (Green): Ray partially reflected, according to law of reflection. The transmitted part is subject to refraction. (Orange): Ray with an angle of incidence larger than $\theta_{crit}$, cannot be transmitted and experiences Total Internal Reflection*

Increasing the angle of incidence above normal will ultimately result in a wavelength shift at the transmission spectrum of the filter. This shift is dependent upon the filter design, and is therefore modeled accordingly, as it varies across filters. Each dichroic mirror is characterized by a certain value called Filter Effective Index ( $n_{eff}$ ), among others, which is used to calculate the, angle of incidence dependent, wavelength shift of its spectral features. The Filter Effective Index describes the entire filter, including the coatings on both sides as well as the substrate between

the coatings. The shift of each spectral component at the transmission spectrum of a dichroic mirror, as a function of the angle of incidence, can be calculated using the following formula:

$$\lambda(\theta)=\lambda_0\sqrt{1-\left(\frac{\sin(\theta)}{n_{eff}}\right)^2} \quad ,$$

where $n_{eff}$ is the effective index of refraction, which varies with polarization, and $\lambda_0$ is the wavelength of the spectral feature of interest at normal incidence.

Using this formula, it is possible to calculate the shift of a certain wavelength at the transmission spectrum of a certain filer, as a function of a given angle of incidence. A few interesting characteristics, concerning the behavior of the filter at non-normal angles of incidence, derive from this equation.

Given that the angle $\theta$ is, apparently, at least 0˚ and less than 90˚, the sinus of that angle can vary from 0 to less than 1. The factor $\left(\sin(\theta)/n_{eff}\right)^2$ will also always be positive and less than 1, since $n_{eff}$ is a value larger than 1. The factor $\sqrt{1-\left(\sin(\theta)/n_{eff}\right)^2}$ is consequently a positive number between 0 and 1, with the case of it being equal to 1 referring to the normal angle of incidence, where $\theta=0$ and $\lambda(\theta)=\lambda_0$ .

Since the factor of $\lambda_0$ is at most 1, each spectral component will eventually shift towards shorter wavelengths as the deviation from the normal angle of incidence gets bigger. In fact, as the angle of incidence increases, the factor $\sqrt{1-\left(\sin(\theta)/n_{eff}\right)^2}$ decreases accordingly, resulting in a greater shift towards shorter wavelength values.

For a given filter and a given angle of incidence, though, the factor $\sqrt{1-\left(\sin(\theta)/n_{eff}\right)^2}$ is a fixed number.

Let $a=\sqrt{1-\left(\sin(\theta)/n_{eff}\right)^2}$ .

Then, the shift of a certain spectral feature, corresponding to a wavelength $\lambda_0$ at normal incidence and $\lambda(\theta)$ at an angle of incidence equal to $\theta$, can be calculated as

$$\lambda_0 - \lambda(\theta) = \lambda_0(1-\alpha) \quad .$$

As this equation implies, the shift of each spectral component is, apparently, relative to $\lambda_0$. Consequently, larger wavelengths experience larger deviation than shorter wavelengths.

This formula also describes the effect of the Filter Effective Index ( $n_{eff}$ ) of a filter, which ultimately defines its angle sensitivity, as a greater $n_{eff}$ will actually reduce the impact of the angle of incidence.

Eventually, the central wavelength of a pass-band in a dichroic filter shifts towards shorter wavelengths with an increase in the angle of incidence. The amount of shift is dependent upon the angle of incidence and the Effective Index of the filter ( $n_{eff}$ ), yet relative to wavelength ( $\lambda_0$ ). This is better illustrated in the following Figure:

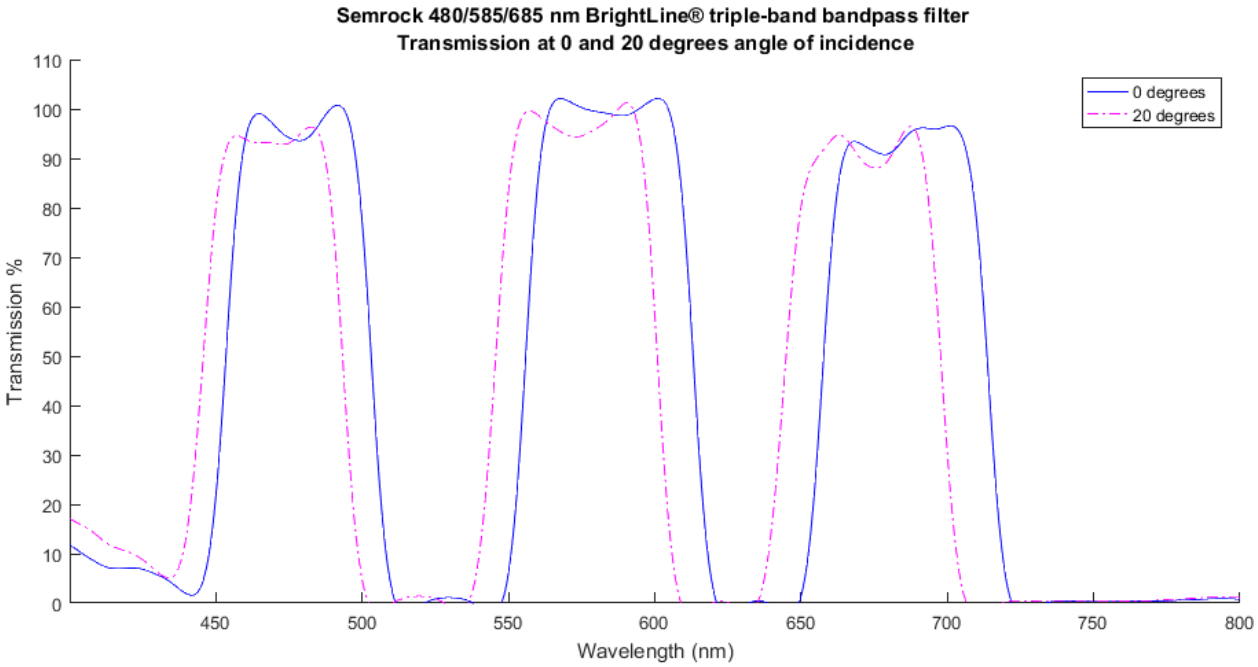

*[Figure 2.6] Spectral Response of a rotating dichroic band pass filter. Transmission spectrum of the Semrock 480/585/685 nm BrightLine® triple-band bandpass filter as measured using a USB2000 Fiber Optic Spectrometer under 0 and 20 degrees angle of incidence. Horizontal axis represents wavelength. Vertical axis corresponds to transmission ratio.*

At this particular filter, the central wavelengths of the three pass-bands shifted from 485nm, 585nm, and 685nm at normal angle of incidence, to approximately 469nm, 574nm and 672nm respectively at an angle of 20 degrees. Using the corresponding formula presented above, the expected central wavelengths are calculated to be at 472nm, 575nm and 673nm.

As the angle of incidence increasingly deviates from normal, two distinct spectra emerge, one for s-polarized light, whose electric field is perpendicular to the plane of incidence, and one for p-polarized light, with its electric field along the plane of incidence. The exact effect of polarization varies greatly with wavelength and with the particular filter design. The transmission of the average unpolarized light, as shown in *Figure 2.6*, as well as the bandwidth of pass-bands slightly decrease as the angle of incidence increases. The polarization effects evidently course a harsh distortion at great angles.

Dichroic filters are generally considered to be non-tunable, as their exact specifications are determined during production, while their intrinsic angle sensitivity is often perceived as a defective characteristic. Although, by being able to model and predict the filter's behavior at varying angles of incidence of light, it is possible to use this distinctive attribute in order to selectively shift transmission bands across the spectrum. Therefore, a dichroic mirror tilted at will, can eventually act as a tunable band-pass filter.

# Chapter 3:

# Application Principle and Development

# 3. Application Principle and Development

## 3.1 Application Principle

This study's principle lies on testing the feasibility of creating a spectral imaging system, that scans across the electromagnetic spectrum utilizing a single rotating dichroic mirror as a tunable filter. As presented, dichroic filters have the unique ability to shift their spectral features as the angle of incidence changes. Therefore, it is possible to selectively tune the central wavelength of a transmission band on a band pass dichroic filter, by adjusting the angle at which light is incident on the filter.

In this particular design, a triple-band bandpass dichroic filter is mounted in front of a CMOS color camera. Having three distinct pass bands, instead of only one, provides the advantage of scanning a broader part of the spectrum, while obtaining information for more spectral bands, over the same acquisition time and rotation angle. Scanning the same amount of spectral bands using a simple band-pass filter would require triple acquisition time, as well as triple rotation, which can be practically impossible depending on the filter and the system characteristics. The spectral resolution of this design, though, is not solely dependent on the filter. The color sensitivity of the camera -that can detect three color channels- is also vital, in order to obtain spatial information from three spectral bands simultaneously.

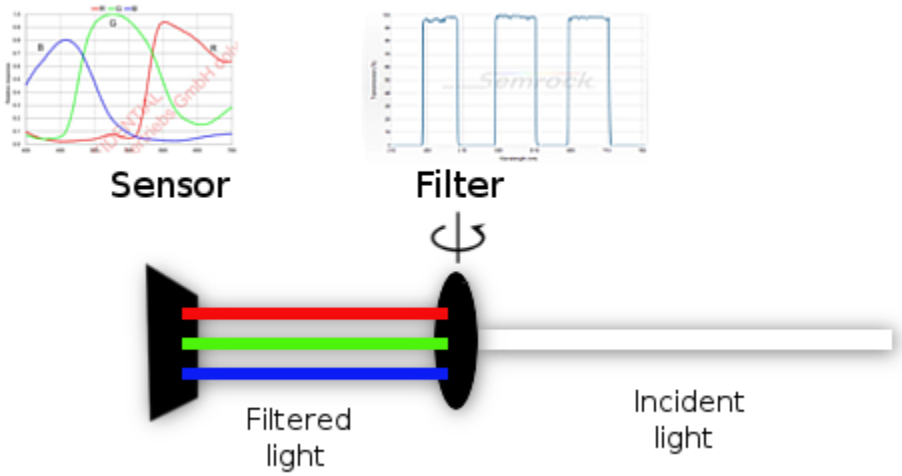


*[Figure 3.1] Optical Filter with three pass-bands, camera with three color channels*

As each 2-D spectral image of the Spectral Cube illustrates the intensity of light of a specific frequency across the scene, the desired spatial information can be entirely presented in grayscale. Therefore, there is no need for the camera of a spectral imaging system to be color sensitive, as long as the detected light at each exposure corresponds to a single spectral band. By using a color camera, namely a sensor that can distinctively obtain spatial information in three individual spectral channels, all three pass bands of the filter can be captured simultaneously and processed separately.

This way, it is possible for the proposed design to effectively capture wavelength dependent spatial information, for instance in 24 distinct spectral bands after 8 exposures. Each exposure corresponds to a certain deviation from the normal angle of incidence of light, as the filter rotates, in this case from 0 to 40 degrees with 5 degree steps. The rotation of the filter is achieved using a low power stepper motor, driven with an arduino, in order to achieve precise steps. Light is concentrated on the sensor using a C-mount Fixed Focal Length lens. The whole system is contained in a black enclosure that was created in a 3-D printer and can be controlled using a computer with the accompanying software, developed in Python.

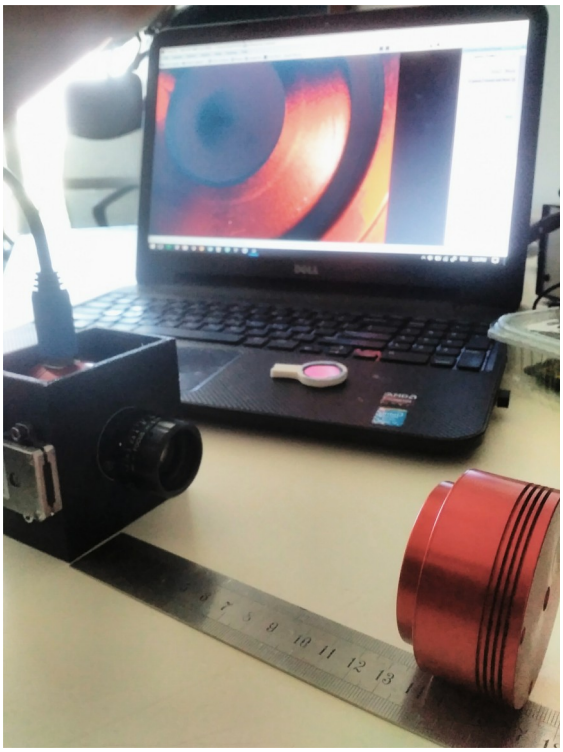

*[Figure 3.2] Actual photo of the proposed device*

## 3.2 Hardware

The proposed spectral imaging system consists of three optical elements and a scanning mechanism. The optical elements include:

- a camera, that is used to capture spatial information,
- a dichroic filter, that transmits the desired spectral components selectively and
- a Fixed Focal Length lens, used to concentrate light to the sensor.

The other elemental components of this design are:

- the stepper motor, that is used to rotate the filter, and
- the arduino, that is utilized to drive the motor

A computer is used to manipulate the camera and the arduino, as well as to process and store the acquired images.

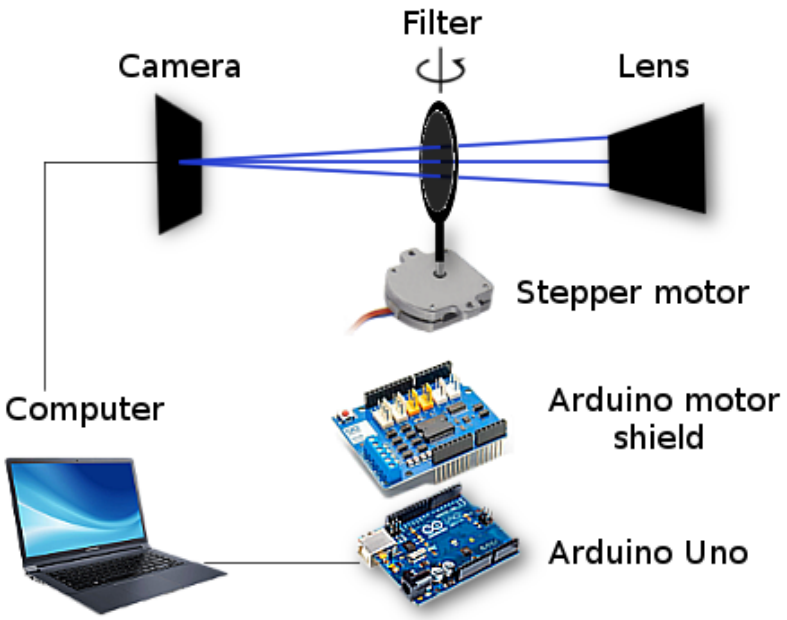


*[Figure 3.3] Diagram of the Proposed System*

### 3.2.1 Camera

The camera used in this particular design is the ASI178MC color camera from ZWO. This particular camera is characterized by very low read noise and is therefore especially suitable for demanding applications, including microscopy and high resolution imaging, among others. It utilizes a Back-illuminated CMOS Image Sensor at the size of 1/1.8″ with 6.4 Mpixels and is equipped with a 14bit Analog to Digital Converter (ADC).

*[Figure 3.4] ZWO ASI178MC (color) camera*

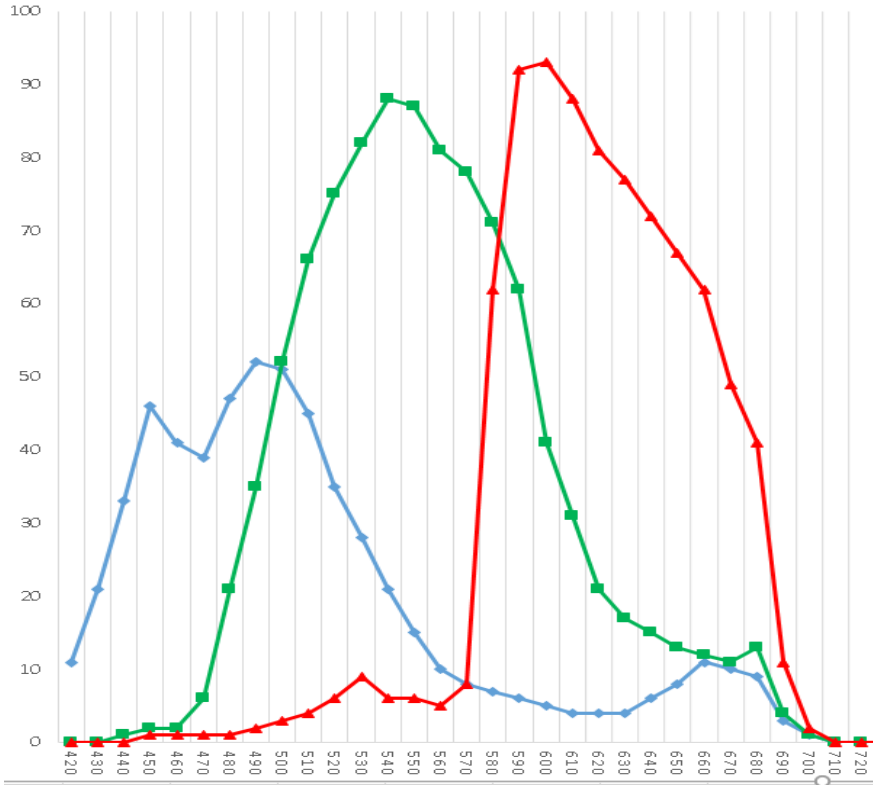


*[Figure 3.5] Spectral Response of ZWO ASI178MC (color) camera. Horizontal axis represents wavelength, vertical axis illustrates transmission ratio.*

It supports USB 3 interface, which is used by the computer to power and manipulate the camera, as well as to receive the acquired data. The settings for each capture can be programmatically set at will. The exposure can vary from 32μs to 1000s, while the resolution of the acquired images can be up to 3096*2080 pixels. It can also achieve a maximum of 60 Frames Per Second (FPS) at full resolution.

The sensor is covered with an Anti-Reflection (AR) and Infrared Cut (IR-Cut) protect window, that ultimately limits the spectral response of the camera to the visible region, from 400nm to 700nm, while eliminating all other wavelengths.

### 3.2.2 Optical Filter

The optical filter in this design is of vast importance, as it primarily dictates the spectral response of the system. The filter used is the 480/585/685 nm BrightLine® triple-band dichroic bandpass filter from Semrock. Its frequency response at normal angle of incidence is presented below:

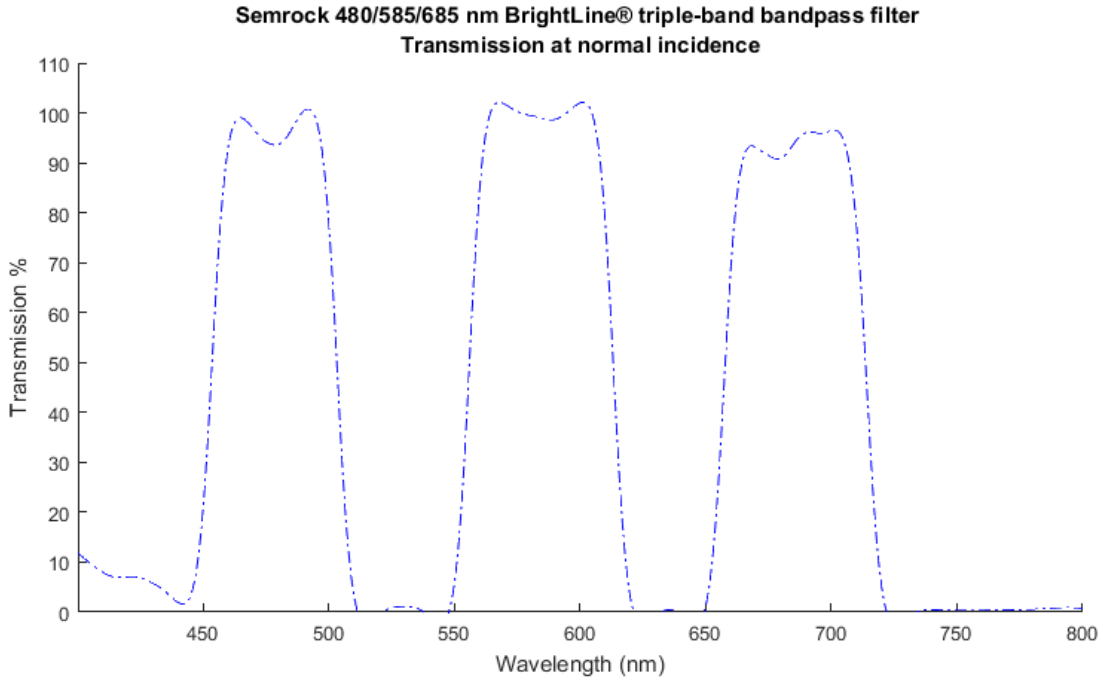


*[Figure 3.6] Transmission spectrum of the 480/585/685 nm BrightLine® at normal incidence. Measured using a USB2000 Fiber Optic Spectrometer, at normal incidence. The vertical axis corresponds to transmission ratio and the horizontal axis represents wavelength.*

This particular filter has three pass bands, having central wavelengths at

- 480nm, with nominal FWHM Bandwidth of 49.9nm,
- 585nm, with nominal FWHM Bandwidth of 57.6nm and
- 685nm, with nominal FWHM Bandwidth of 57.2nm

respectively, while it also transmits a portion of Infrared light which, although, is later rejected from the coating of the camera.

This filter has a nominal tolerance in the angle of incidence of 0 ± 5 degrees and Cone Half-angle 7 degrees. Its effective index of refraction is $n_{eff}=1.82$ . As the latter characteristics suggest, any deviation larger than 5 degrees from the normal angle of incidence is going to result in a considerable amount of shift in the spectral features of this filter. This dictates its accountability for this particular application. The distribution of the central wavelengths of each FWHM pass-band observed after rotating the filter from 0 to 60 degrees with 5 degrees interval, is presented in the following figures:

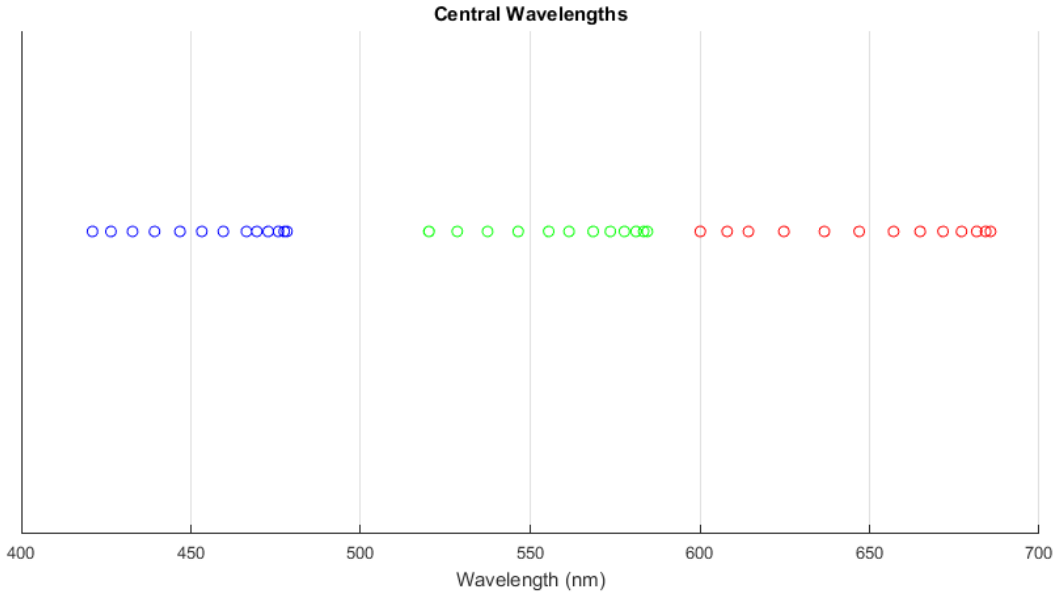


*[Figure 3.7] Distribution of the Central Wavelengths of each pass-band of the 480/585/685 nm BrightLine® upon rotation from 0 to 60 degrees with 5 degree steps. The horizontal axis represents*

*wavelength. Each rotational step produces three new central wavelengths, one in each group, on a slightly shorter wavelength than the previous step.*

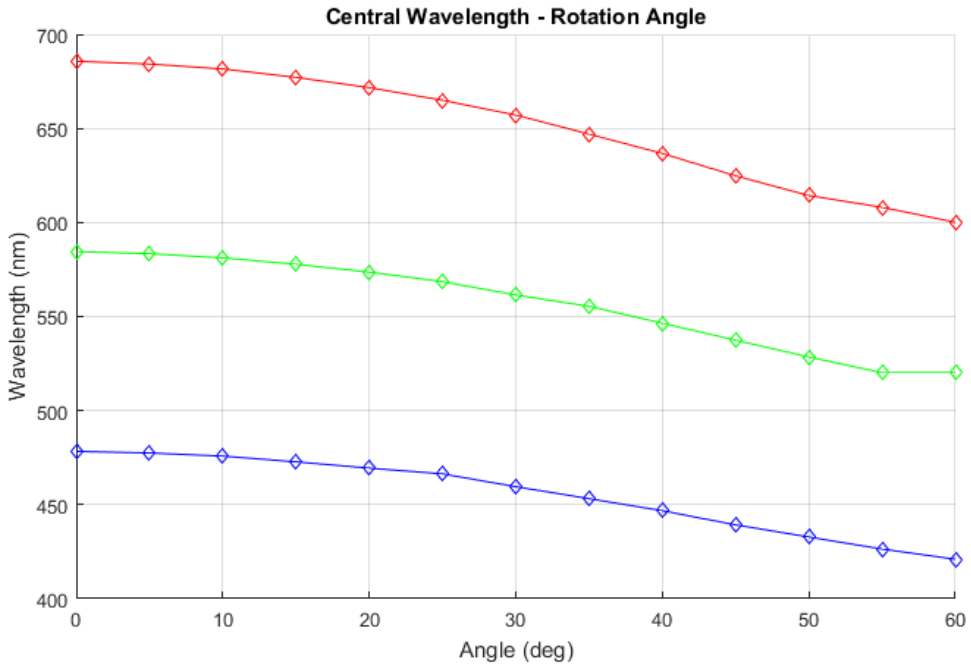


*[Figure 3.8] Central Wavelength shift of the 480/585/685 nm BrightLine® upon rotation from 0 to 60 degrees with 5 degree steps. The vertical axis represents wavelength and the horizontal axis corresponds to the angle of rotation of the filter.*

As illustrated, the 480/585/685 nm BrightLine® triple-band dichroic bandpass filter can be very efficient when utilized as a tunable filter in the visible range, as it can scan across the entire visible range of the electromagnetic spectrum with considerable transmission ratio.

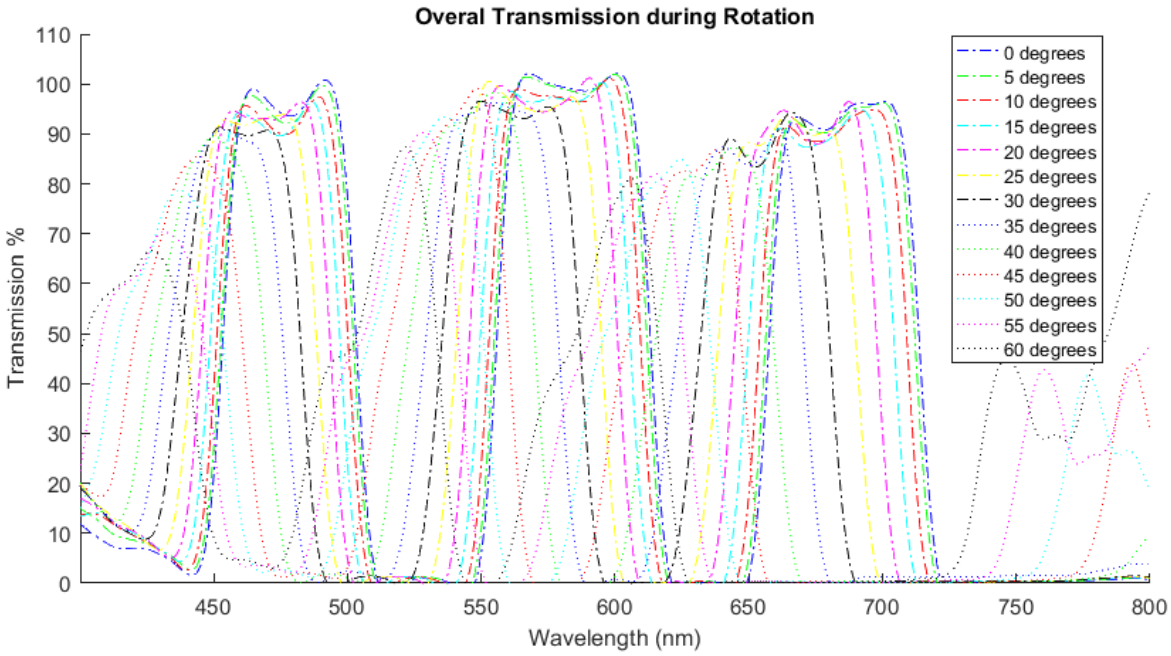


*[Figure 3.9] Total Transmission spectrum of the 480/585/685 nm BrightLine® upon rotation from 0 to 60 degrees with 5 degree steps. The horizontal axis represents wavelength and the vertical corresponds to transmission ratio. Each rotational step produces three new pass-bands with slightly shorter central wavelength and lower transmission ratio, than the previous step.*

### 3.2.3 Lens

A C-mount Fixed Focal Length Lens is mounted on the proposed device, in order to concentrate light from the scene onto the camera. The particular Lens used is TECHSPEC® COMPACT FIXED FOCAL LENGTH LENS #59-871, 25mm FL, f/1.4 from Edmund Optics. As its name suggests, this Lens has a focal length of 25mm, with an aperture of f/1.4.

This lens is also equipped with a broadband anti-reflection coating, in order to increase transmission in the visible spectrum. It provides the proposed system with a minimum working distance of 100mm and 16.1 degrees Field Of View, given that the sensor of the ASI178MC camera is 1/1.8” in size.

### 3.2.4 Motor

Constructing a mechanism that assists the rotational movement of an optical filter as a spectral scanning system, is a highly demanding application, primarily in terms of precision, accuracy, throughput and size. The motor that facilitates this design should be characterized by great precision, in terms of accuracy and repeatability, as well as millisecond response.

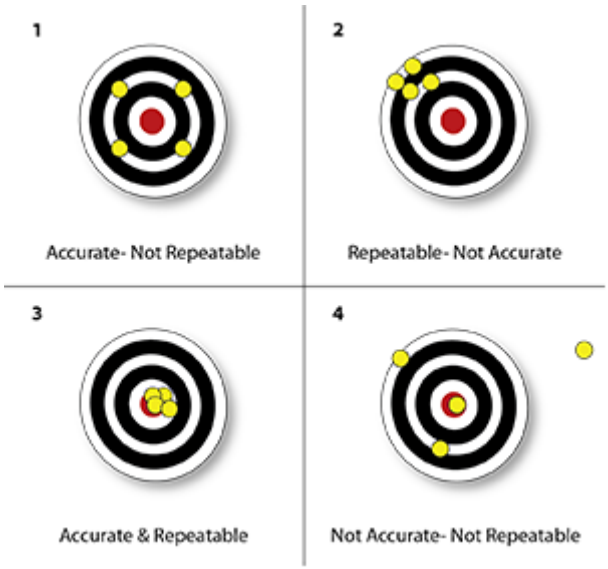


*[Figure 3.10] Precision of a motor, in terms of accuracy and repeatability.*

Another important characteristic of an accountable motor, is low power consumption, in order to avoid the need of external driver, high power supply or batteries, as this would reduce usability, while increasing cost, size and weight. In addition, for better user experience, the motor should be quiet during operation, while its physical characteristics are also important, as it should be light and small, in order to construct a portable device.

Stepper motors meet most of the requirements of this particular application, with their high step angle precision, step resolution and fast response serving as their main features. This type of brushless DC electric motor, has another exceptional advantage, which is its inherent ability to control position, as stepper motors have built-in output steps. Therefore the driver, namely the Arduino in this particular design, is able to calculate the position of the motor at any given time during operation, as long as it knows its exact position on power up. For this reason, in most applications that utilize stepper motors, including this study, the controller activates the motor and turns it into a known position on power up.

The high step angle precision of stepper motors can also be further increased, using microstepping. Microstepping, is a way of performing steps smaller than the nominal step angle, by sending sine and cosine waveforms to the coils inside the motor. In most cases, this allows stepper motors to run smoother and more accurately.

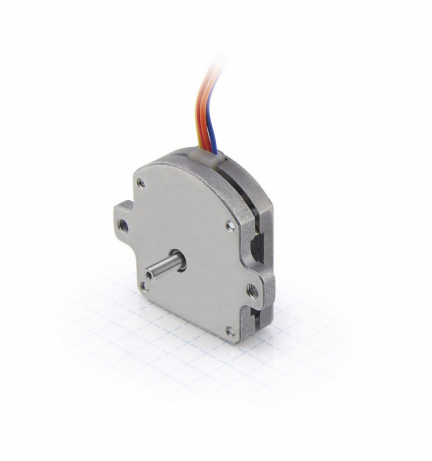

*[Figure 3.11] Nanotec STF2818X0504-A - Ultraflat Stepper Motor*

The motor used in this particular design is the STF2818X0504-A Stepper Motor from Nanotech. Its ultra-flat design (9.5mm height) and high torque, make it especially suitable for this application, while it has a full step angle of 1.8 degrees. This bipolar stepper motor can be driven with 1.85 Volts, demanding 500mA of current per phase, a power consumption that an arduino powered by USB with 5V, 500mA is able to compensate, with the use of the appropriate shield. Therefore, it perfectly meets all the application requirements regarding its physical and technical characteristics, while it is also silent during operation. A 3-D printed holder for the optical filter is mounted on the shaft of this motor, for the needs of this application.

### 3.2.5 Arduino with Motor Shield

For the development process, an Arduino UNO equipped with an Arduino Motor Shield serves as the motor driver. It is powered and controlled from the computer using USB 2 interface. Based on the ATmega328P and a 16 MHz quartz crystal, it can easily compensate the throughput requirements as the motor driver in this application.


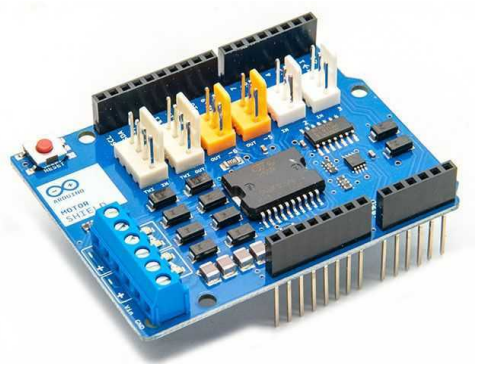

*[Figure 3.12] (Left) Arduino Uno*

*[Figure 3.13] (Right) Arduino Motor Shield*

Powered with USB, the arduino has an input voltage of 5 Volts with a maximum of 500mA current drain limited by the USB Interface. When powered by external supply, using the barel power connector, power is limited by the on board 5V regulator, restricting current drain to a maximum of 1A. Its digital Input-Output pins (IO pins) can provide 5 Volts with a maximum of 20mA per pin, which, although, is not enough for the STF2818X0504-A Stepper Motor to perform efficiently, as each phase would require 500mA of current. In order to unlock the full potential of the motor, it is essential to use the Arduino Motor Shield.

The Motor Shield is based on the dual full-bridge driver L298 and designed to drive inductive loads such as relays, solenoids, DC and bipolar stepper motors, through two independent channels. It can operate with an input Voltage of 5V to 12V, providing up to 2A per channel, or 4A in a single channel, when powered with external supply. This shield also provides other features, including current sensing, so that is possible to measure the power drain of the motor, as well as two Pulse With Modulation outputs that can assist microstepping by sending sinus and cosine waves to the stepper motor coils.

Without the use of external supply, thus only powered from the computer through the Arduino, this motor shield is eventually able to drive the STF2818X0504-A bipolar stepper motor with great precision of 1.8degrees per step, or 200 steps per revolution at full speed, without microstepping.

## 3.3 Software

The accompanying software of the proposed spectral imaging device is designed to control the camera and the motor, as well as to process and store the acquired images and provide the User Interface. It is developed in Python and consists of three elementary modules

- ArduinoBackend.py, that implements the serial connection between the arduino and the computer,

- ASICamBackend.py, that assists the communication with the ASI178MC USB 3 color camera and grants access into its settings and controls and

- ImageProcessing.py, which processes the acquired images and constructs the corresponding spectral cube,

along with the Graphical User Interface (GUI) Page, that ultimately controls the device and presents the acquired data and results to the user.

The micro-controller is programmed to serve as the motor driver, using the Arduino programming language.

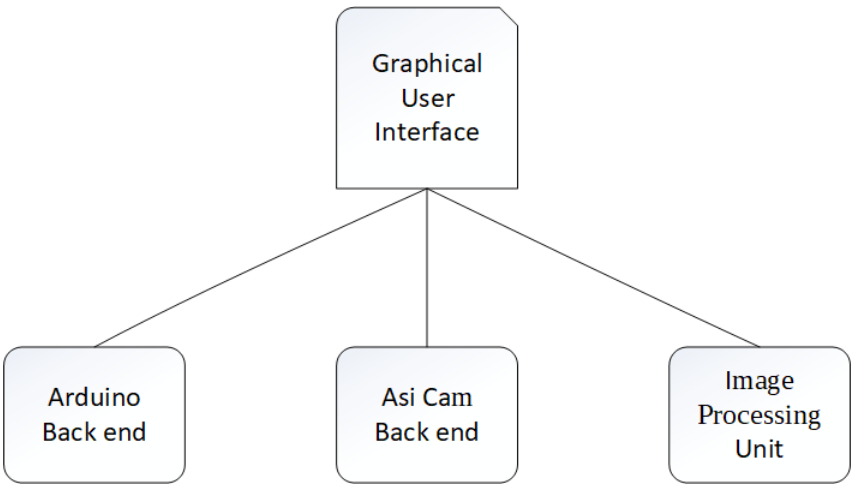


*[Figure 3.13] Structure of the Software accompanying the proposed device.*

### 3.3.1 Arduino Back-end

The Arduino is able to drive the stepper motor used in this application, using the Arduino Stepper library [48]. It also provides visual information about the state of both the motor and the connection with the accompanying application, by powering the corresponding Light Emitting Diodes (LEDs).

On power up, the Arduino is programmed to move the motor until it locates its position, with the use of an optocoupler. The optocoupler actually serves as an optical switch, that detects whether the motor stands in its initial position. During operation, this algorithm is able to command the STF2818X0504-A bipolar stepper motor to rotate continuously in both directions, and even perform any combination of single steps, as small as 1.8 degrees, when instructed accordingly. The communication with the GUI is established using the Serial Port and the Serial.read() function, that receives a single character from the port, when available. Reading the serial input as a stream of individual characters, instead of a single string or numbers, significantly shortens the time needed between the action of the user and the actual movement of the motor.

On the other hand, in service of the User Interface, ArduinoBackend.py is responsible for the communication with the Arduino, which controls the motor. Essentially, this module scans across the serial ports of the computer, searching for a potential connection with the Arduino. It is also able to setup the serial connection, if requested. This module ultimately governs the communication with the micro-controller, sending the appropriate messages, while monitoring for errors. This communication is established using the serial port, at 115200 Baud Rate, namely 115200 bits per second, while the commands for the Arduino are encoded in single characters.

### 3.3.2 ASI Cam Back-end

ASICamBackend.py is the camera control module of this system. It uses the official ZWO Asi native driver [49] and python-zwoasi [50], which is a python library based on the official ASICamera2 Software Development Kit (SDK) Revision:2,0 2016.12.9 from ZWO. This module can read and set any of the controllable settings of the camera, including gain, exposure time, white balance and brightness, as well as capture images and video.

Essentially, this module detects any ZWO Asi cameras connected to the computer. When a camera is found, it automatically sets up the connection and scans the camera’s properties and

settings. Thereby, it is able to capture a single image or video at any format and resolution provided. ASI178MC color camera provides various image formats including RAW8, RAW16 and RGB24, that can be saved as any desired file type, for instance PNG, JPEG and TIFF. Accordingly, when in video mode, this camera is able to feed this module with up to 60 Frames Per Second (FPS) at full resolution. The maximum resolution available, is 3629*2175 pixels.

For the needs of this application, the images are captured with RGB 24 format and saved as Portable Network Graphics (PNG) files. PNG is especially selected, as it is a lossless image compression format. Evidently, the image resolution has a large effect on the processing time needed for the construction of the spectral cube, as the higher the resolution of an image, the more time it takes to be processed.

### 3.3.3 Image Processing Unit

ImageProcessing.py handles the image processing required to construct the Spectral Cube. The acquired images are essentially transformed, in order to compensate for the spectral response of the filter and the camera at each distinct filter angle. The spatial information of each of the three individual channels of the camera is, then, stored as a 2-D gray-scale image of the spectral cube, corresponding to a particular wavelength.

Essentially, this module is able to read a given RGB image and process each of the three channels individually. It calculates the corresponding wavelengths for the three images that emerge, according to the position of the filter upon acquisition, and then applies any specific transformation required. Each individual grayscale image is stored as a python Object, containing the actual image as a numpy array, along with its corresponding wavelength, representing the 2-D image I(x, y) of the given wavelength (λ) in the spectral cube.

The complete spectral cube is stored both as a set of PNG image files, and locally as a set of Objects, so that it is easily accessible as soon as it is constructed, as well as after the examination has been completed. The spectrum of each pixel can be accessed through the User Interface and presented in the form of a matlab figure, using the python matlpotlib library **[51]**.

### 3.3.4 Graphical User Interface

The GUI of this application allows the user to watch the video feed of the camera, as well as to acquire the complete spectral cube of the observed scene, in a completely automated manner. In order for this application to be consistent and responsive, the parallelism between certain processes is indispensable. This parallelism is achieved using threads, a functionality provided by the python Threading library[52].

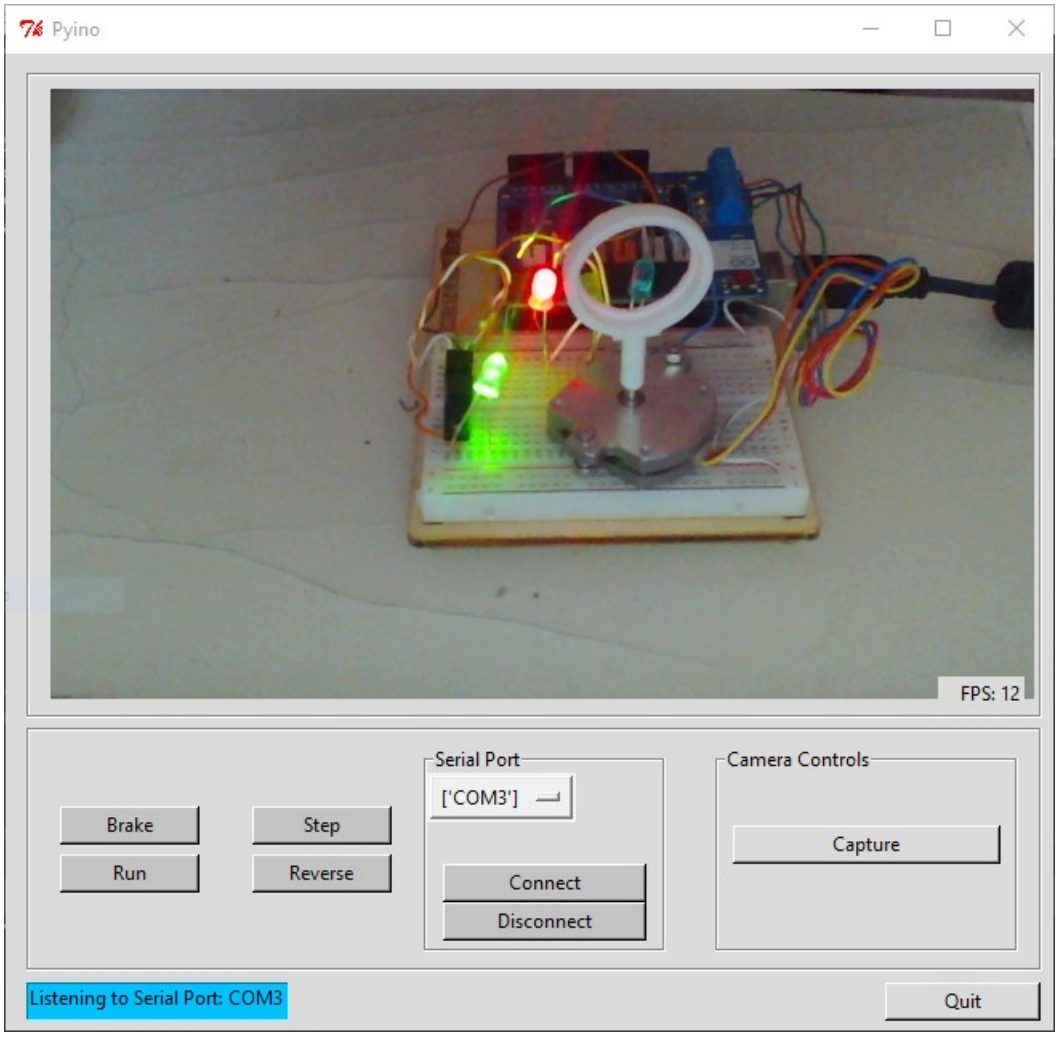


*[Figure 3.14] Image of the Graphical User Interface of the proposed system*

Initially, in this screen the user can see whether a serial connection is available and can eventually establish communication with the Arduino. The connection is accomplished using the

ArduinoBackend.py, that is designed to encode and send any commands to the microcontroller in the device. The Interface also provides information about the serial connection status.

This module also handles the projection of the information captured by the camera, utilizing the ASICamBackend.py. When a ZWO ASI camera is connected to the computer, this module commands the initialization of the camera and starts a video recording. Each frame of the video is stored in a buffer, while a thread responsible for the projection of the video is constantly polling this buffer, searching for new available frames. As soon as a frame is available, it is presented in the screen, using the OpenCV 2 python library **[53]**. This implements real time video streaming from the camera to the computer screen, so that the user can adjust the device as desired.

This User Interface, additionally, provides the functionality to perform a full image spectral scan, pushing a single button. As soon as the Capture button is pressed, the device performs a predefined set of motor steps and image captures. In the following demonstration, each step is equivalent to 5 degrees rotation, resulting in 5 degrees larger deviation from the normal angle that light is incident on the filter. After each exposure, a dedicated thread is assigned to process each of the three color channels individually and add the processed data in the spectral cube, while, at the same time, the system performs the acquisition of the next images.

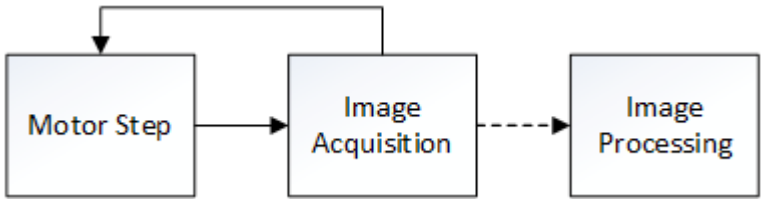


*[Figure 3.15] High level Flowchart of the proposed system.*

In the following demonstration, the motor performs 8 sequential steps of 5 degrees, thus rotating the filter from 0 to 40 degrees. The device ultimately captures 9 images of 1024*644 pixels, corresponding to the spatial information of 27 individual spectral elements. The entire scan is performed within 10 seconds, while at the same time the Image Processing Unit is constructing the complete spectral cube, consisting of images at 1024*644 pixels resolution. Apparently, the time needed for the information processing to complete, largely depends on the image resolution.

# Chapter 4:

# Observations and Results

# 4. Observations and Results

## 4.1 Observations

The overall results of this design are very inspiring. In this demonstration, the system acquires a spectral image corresponding to 27 individual spectral channels, in a reasonably short time, covering a reasonable portion of the visible spectrum. Apparently, the number of distinct wavelengths that this system obtains, can be selectively increased greatly, by decreasing the amount of rotation that the filter performs at each step. The proposed system can, ultimately, be considered a hyperspectral imaging device. The total transmission of the filter, after rotating from 0 to 40 degrees with 5 degree steps, is presented in the following figure:

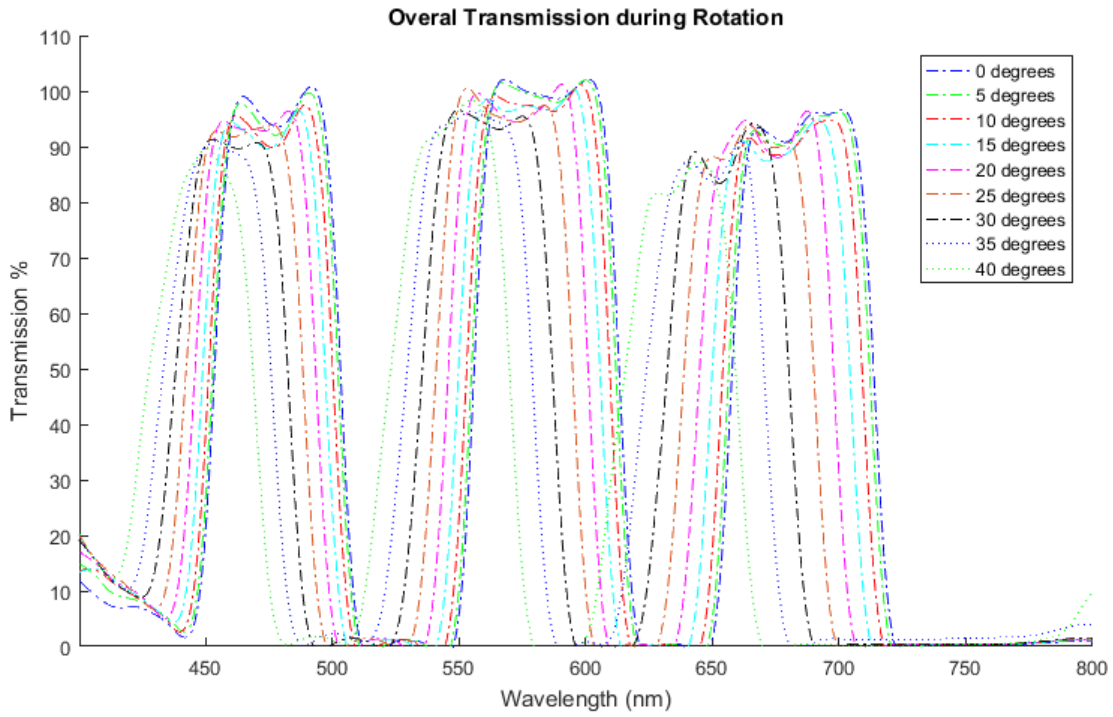


*[Figure 4.1] Transmission of the Semrock 480/585/685 nm BrightLine® during rotation from 0 to 40 degrees. Transmission spectrum, as measured using a USB2000 Fiber Optic Spectrometer from 0 to 40 degrees rotation with 5 degree intervals. Horizontal axis represents wavelength and vertical axis represents transmission ratio*

The following table shows the corresponding central wavelength of each pass-band, as calculated according to the FWHM, in the same setup :

| **Degrees of filter Rotation** | **Central Wavelengths** | | |
|---|---|---|---|
| | **Pass-Band 1** | **Pass-Band 2** | **Pass-Band 3** |
| 0 | 478 | 584 | 685 |
| 5 | 477 | 583 | 684 |
| 10 | 475 | 581 | 681 |
| 15 | 472 | 577 | 677 |
| 20 | 469 | 573 | 671 |
| 25 | 466 | 568 | 664 |
| 30 | 459 | 561 | 657 |
| 35 | 453 | 555 | 647 |
| 40 | 446 | 546 | 636 |

Eventually, the behavior of the filter's spectral response during rotation is, in fact, accurately described by the equation

$$\lambda(\theta)=\lambda_0\sqrt{1-\left(\frac{\sin(\theta)}{n_{eff}}\right)^2}$$

The observed shift in each spectral feature of the 480/585/685 nm BrightLine® triple-band dichroic bandpass filter from Semrock, with an Effective Index $n_{eff}=1.82$ , accurately corresponds to the shift calculated using the above formula. This is better illustrated in the following Figure:

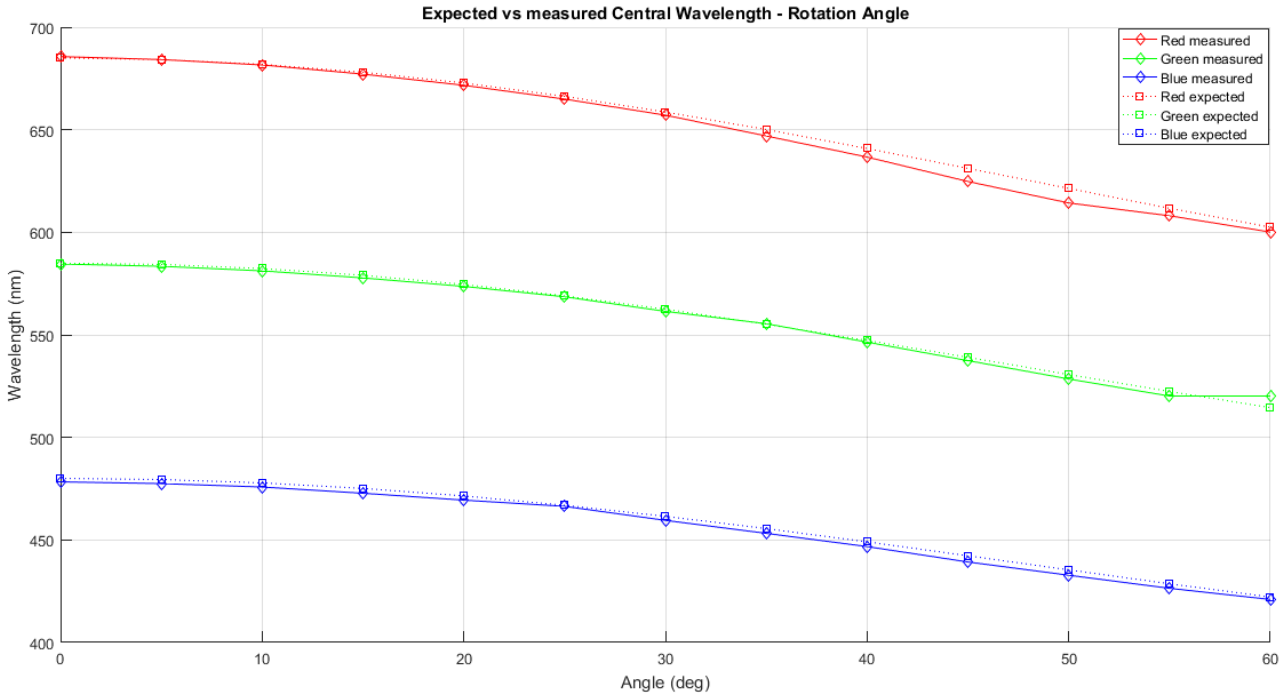


*[Figure 4.2] Expected vs measured Central Wavelengths. The central wavelength of each pass band of the Semrock 480/585/685 nm BrightLine® triple-band dichroic bandpass filter, as measured (solid line) according to the FWHM and calculated using the corresponding formula (dotted line) for 0 to 40 degrees rotation in 5 degree steps. Horizontal axis represents rotation angle and vertical axis represents wavelength.*

Ultimately, the proposed system is able to accurately evaluate the spectrum of each pixel and construct the Spectral Cube of the image. In this particular demonstration, the following target is examined:

*[Figure 4.3] Target examined during demonstration*

The Spectral Cube, as evaluated from this setup, consists of 27 images, each one corresponding to a certain spectral band, approximately 50 nm wide.


*[Figure 4.3] The Spectral Cube, as evaluated using the proposed system*

Eventually, the proposed system is able to identify the spectral composition of light reflecting from the target at each pixel. For instance, the red colored checker appears brighter at longer wavelengths, whereas the dark and light blue checkers are brighter at lower wavelengths. Accordingly, the intensity of light reflecting from the green checker is larger above 500nm and below 600nm. The spectrum of each pixel can also be accessed from the GUI of this application and presented in the form of a graph for easier examination.

By double-clicking at a certain pixel of the image, the spectrum of the selected pixel is presented to the user. For example, the following image shows the spectrum of the white checker.

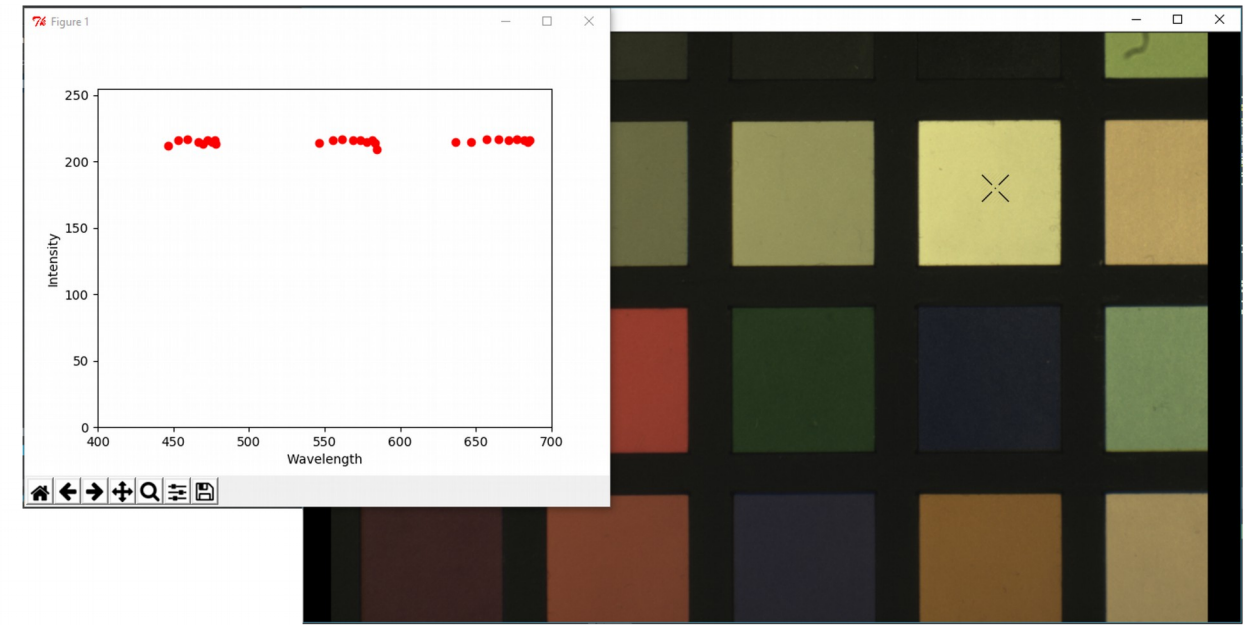


*[Figure 4.5] Spectrum of a white checker, as evaluated using the proposed system*

Similarly, the spectrum of the red checker denotes that light is more intense around 650 nm:

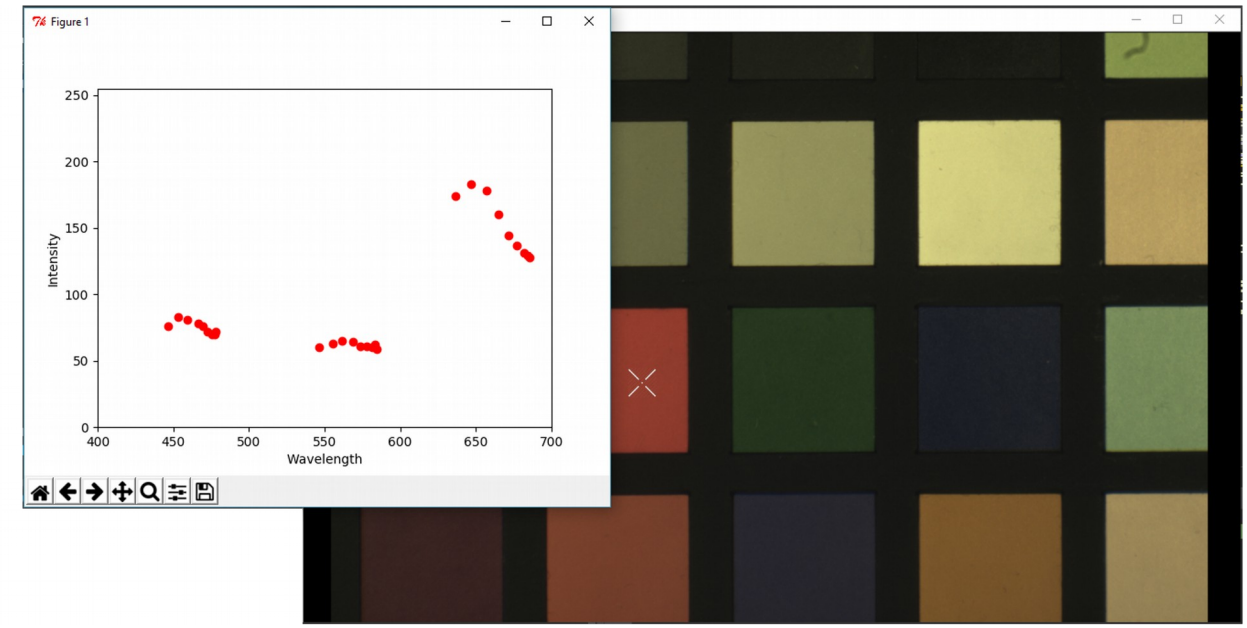


*[Figure 4.6] The Spectrum of a red checker, as evaluated using the proposed system*

## 4.2 Considerations

Despite the significant advantages, there are several aspects in the proposed design, that essentially have to be taken into account. These include various artifact inducing factors, for instance low transmission ratio of the filter at large angles, movement artifacts and cross-talk, among others. Calibration of the system is needed, in order to eliminate the effect of such factors, leading to the construction of a Spectral Cube that encompasses legitimate information.

The transmission ratio of the filter, evidently, decreases slightly with an increase in the angle of incidence. In large angles, though, namely exceeding 40 degrees in this particular setup, it experiences a significant drop, thus not being able to provide adequate information to the camera. The total amount of the rotation possible, is also bound from the system's physical and optical characteristics. According to the Lens used, the Sensor must have a certain distance from the Lens, therefore establishing a strict constraint to the size of the Filter, that lies between the two, as well as to the maximum angle of rotation permitted. This, apparently, translates into a limitation regarding the maximum number of distinct wavelengths that this system can distinguish. Respectively, restricted rotation also corresponds to a smaller overall shift of the filter's spectral features.

Additionally, in order to provide legitimate information, this system is calibrated to compensate for the spectral response of the particular filter and the sensor used. The drop in the transmission ratio of the filter, as well as the shift of its spectral features due to the non-normal angle of incidence, are not identical at each transmission band. Also, the spectral response of the camera is not even across the visible part of the electromagnetic spectrum. Therefore, each observed channel is specifically transformed, in order to reconstruct the actual information it carries. Still, unmixing of the color channels of the camera is required to create a cross-talk free system and, therefore, provide more accurate results.

Furthermore, changing the angle of incidence fundamentally results in a different angle of refraction. Eventually, this is observed as a shift in the spatial information of the image, apparently in space, proportionate to the non-normal angle that light is incident on the filter. This factor has to be considered when aligning the acquired 2-D images to construct the spectral cube.

As a device that utilizes the wavelength-scan method to acquire spectral images, the proposed system is also subject to movement artifacts. As multiple exposures of the same scene are required in order to obtain the entire spectral cube, movement in the scene and, especially, movement of the examined object can induce artifacts in the image. In order for this design to produce legitimate results, the examined target has to be stable during acquisition. Otherwise, further processing of the acquired images is needed, in spite of reducing the impact of movement artifacts in the spectral image.

## 4.3 Advantages of the proposed method

Ultimately, this method of spectral imaging is highly promising, while designs such as the one proposed in this study, can be very efficient and profoundly scalable. Using a rotating dichroic band pass filter as a tunable filter, can eventually reduce the size and cost of a spectral imaging system, while greatly increasing flexibility.

Utilized as tunable filters, dichroic mirrors outperform both LCTF and AOTF designs, when carefully selected and tuned to match the application requirements, as they can achieve significantly higher transmission ratio. In comparison with the filter wheel approach, the proposed setup makes optimal reusability of the optical elements used to distinguish spectral information, thus reducing size, cost, weight and complexity, while also being largely scalable.

Being properly designed, this particular setup can be precisely tuned to match virtually any specific requirements of a spectral imaging application in the visible region. By adjusting the steps of the motor, it is possible to tune the system to provide exactly the spectral information needed. Eventually, the number of distinct spectral components being observed, as well as their exact position on the spectrum can be changed at will, thus providing designs based on this method of spectral imaging with characteristic intrinsic flexibility.

While the spectral resolution of the proposed setup is largely scalable, no compromise has been made in the spatial resolution. In contrast to time-scan methods of spectral imaging, the proposed design captures spatial information from each spectral component of interest using the entire surface of the sensor. Therefore, the spatial resolution of such devices fundamentally depends on the properties of the sensor.

An increase in the spectral resolution of this system, would result in larger acquisition and processing time, while increased spatial resolution would only affect processing time. When the motor is carefully selected and controlled, though, the acquisition time is virtually only limited by the frame rate of the camera and the physical limitations of the motor. Consequently, this method of spectral imaging is also characterized by a relatively short acquisition time. An important factor of the short acquisition time in the proposed design, apparently, is the concurrent observation of three individual spectral channels. The time needed for image processing, on the other hand, has been greatly reduced using multi-threading, thus inducing parallelism to this time consuming process.

## 4.4 Future Work

Ultimately, the proposed spectral imaging system has proved to be very efficient, while optimizing reusability of optical elements and flexibility. Utilizing rotating dichroic band pass filters as tunable filters can result to smaller, lighter and cheaper spectral imaging devices, without compromising spectral or spatial resolution.

Eventually, the creation of such portable and accessible spectral imaging devices is imminent. When the motor and the filter are properly selected and the accompanying software makes use of the full potential of the elements it controls, namely the camera and the motor, designs like the one proposed are able to assist a full examination and acquisition of a spectral image in a very short time. In that case, depending on the spatial and the spectral resolution desired, the examination time can potentially be limited down to a fraction of a second. Further optimization of the image processing operation, could result in a real time spectral imaging device with remarkable scalability and compact design.

The physical characteristics of devices that materialize this method of spectral imaging can also be optimized, with the use of smaller, dedicated elements. The use of a smaller sensor and optical filter can, in fact, increase the maximum spectral resolution of the device, as the filter could practically rotate to larger angles. Potentially, a rotating bandpass dichroic filter could even be used individually, as a tunable filter that assists spectral imaging on virtually any commercial camera.

# References


[1] Imaging in Dermatology 1st Edition Editors: Michael Hamblin Pinar Avci Gaurav Gupta eBook ISBN: 9780128028599 Imprint: Academic Press Published Date: 11th August 2016.

[2] Teena M., Manickavasagan A. (2014) Thermal Infrared Imaging. In: Manickavasagan A., Jayasuriya H. (eds) Imaging with Electromagnetic Spectrum. Springer, Berlin, Heidelberg

[3] Andreas Barth, Infrared spectroscopy of proteins, In Biochimica et Biophysica Acta (BBA) - Bioenergetics, Volume 1767, Issue 9, 2007, Pages 1073-1101, ISSN 0005-2728

[4] Bioengineering of the Skin: Cutaneous Blood Flow and Erythema, Volume II Enzo Berardesca, Peter Elsner, Howard I. Maibach. ISBN 9780849383717 - CAT# 8371

[5] U. Rubins, J. Spigulis, L. Valeine, and A. Berzina, "Semi-automatic Detection of Skin Malformations by Analysis of Spectral Images," in Clinical and Biomedical Spectroscopy and Imaging III, V. Deckert and N. Ramanujam, eds., Vol. 8798 of SPIE Proceedings (Optical Society of America, 2013), paper 87980S

[6] Thomas F. Carruthers and David H. Reitze, "LIGO: Finally Poised to Catch Elusive Gravitational Waves?," Optics & Photonics News 26(3), 44-51 (2015)

[7] LIGO: the Laser Interferometer Gravitational-Wave Observatory B P Abbott, R Abbott, R Adhikari et.al. 2009 Rep. Prog. Phys. 72 076901 (25pp)

[8] Stuart BH. Infrared Spectroscopy: Fundamentals and Applications. Ando DJ, editor. Chichester: Wiley; 2004.

[9] Smith E, Dent G. Modern Raman Spectroscopy, a Practical Approach. Chichester: Wiley; 2005.

[10] Guolan Lu, Baowei Fei, "Medical hyperspectral imaging: a review," J. Biomed. Opt. 19(1) 010901 (20 January 2014)

[11] Nakamura M., Nishikawa J., Goto A., Nishimura J., Hashimoto S., Okamoto T., Sakaida I., “Usefulness of ultraslim endoscopy with flexible spectral imaging color enhancement for detection of gastric neoplasm: a preliminary study,” J. Gastrointest. Cancer 44(3), 325–328 (2013).10.1007/s12029-013-9500-z

[12] Ramanujan V. K., Ren S., Park S., Farkas D. L., “Non-invasive, Contrast-enhanced Spectral Imaging of Breast Cancer Signatures in Preclinical Animal Models In vivo,”J. Cell Sci. Ther.1(102), 1 (2010).

[13] Marek Elbaum, Alfred W. Kopf, Harold S. Rabinovitz, Richard G.B. Langley, Hideko Kamino, Martin C. Mihm, Arthur J. Sober, Gary L. Peck, Alexandru Bogdan, Dina Gutkowicz-Krusin, Michael Greenebaum, Sunguk Keem, Margaret Oliviero, Steven Wang, Automatic differentiation of melanoma from melanocytic nevi with multispectral digital dermoscopy: A feasibility study, In Journal of the American Academy of Dermatology, Volume 44, Issue 2, Part 1, 2001, Pages 207-218, ISSN 0190-9622

[14] Li Q., He X., Wang Y., Liu H., Xu D., Guo F., “Review of spectral imaging technology in biomedical engineering: achievements and challenges,” J. Biomed. Opt. 18(10), 100901 (2013).10.1117/1.JBO.18.10.100901

[15] Elbaum M., Kopf A. W., Rabinovitz H. S., Langley R. G., Kamino H., Mihm M. C., Jr, Sober A. J., Peck G. L., Bogdan A., Gutkowicz-Krusin D., Greenebaum M., Keem S., Oliviero M., Wang S., “Automatic differentiation of melanoma from melanocytic nevi with multispectral digital dermoscopy: a feasibility study,” J. Am. Acad. Dermatol. 44(2), 207–218 (2001).10.1067/mjd.2001.110395

[16] Fujii H., Yanagisawa T., Mitsui M., Murakami Y., Yamaguchi M., Ohyama N., Abe T., Yokoi I., Matsuoka Y., Kubota Y., "Extraction of acne lesion in acne patients from multispectral images," Conf. Proc. IEEE Eng. Med. Biol. Soc. 2008, 4078–4081 (2008)

[17] Afromowitz M. A., Callis J. B., Heimbach D. M., DeSoto L. A., Norton M. K., "Multispectral imaging of burn wounds: a new clinical instrument for evaluating burn depth," IEEE Trans. Biomed. Eng. 35(10), 842–850 (1988).10.1109/10.7291

[18] Stamatas G. N., Southall M., Kollias N., "In vivo monitoring of cutaneous edema using spectral imaging in the visible and near infrared," J. Invest. Dermatol. 126(8), 1753–1760 (2006).10.1038/sj.jid.5700329

[19] Kapsokalyvas D., Cicchi R., Bruscino N., Alfieri D., Prignano F., Massi D., Lotti T., Pavone F. S., "In-vivo imaging of psoriatic lesions with polarization multispectral dermoscopy and multiphoton microscopy," Biomed. Opt. Express 5(7), 2405–2419 (2014).10.1364/BOE.5.002405

[20] J. Ryan, C. Davis, N. Tufillaro, R. Kudela and B. Gao,"Application of the Hyperspectral Imager for the Coastal Ocean to Phytoplankton Ecology Studies in Monterey Bay, CA, USA", Remote Sens., vol. 6, no. 2, pp.1007-1025, 2014

[21] Z. Xiong, A. Xie, D. Sun, X. Zeng and D. Liu, "Applications of hyperspectral imaging in chicken meat safety and quality detection and evaluation: a review", Crit. Rev. Food Sci. Nutr., vol. 55, no. 9, pp. 1287-1301, 2014

[22] T. Dougher, "Aerial detection of a simulated CO2 leak from a geologic sequestration site using hyperspectral imagery", Int. J. Greenh. Gas Control, vol. 13, pp. 124-137, 2013

[23] Cosentino A: A practical guide to panoramic multispectral imaging. e-Conservation Magazine. 2013, 25: 64-73.

[24] Frey FS, Warda J, American Institute for Conservation of Historic and Artistic Works, Digital Photographic Documentation Task Force: The AIC guide to digital photography and conservation documentation. 2008, Washington, D.C: American Institute for Conservation of Historic and Artistic Works

[25] Zhao Y, Berns RS, Taplin LA, Coddington J: An investigation of multispectral imaging for the mapping of pigments in paintings. Proc. SPIE 6810. 2008, San Jose, CA: Computer Image Analysis in the Study of Art

[26] Kubik M: Chapter 5 hyperspectral imaging: a new technique for the non-invasive study of artworks. Physical Techniques in the Study of Art, Archaeology and Cultural Heritage, volume 2. 2007, Oxford, UK: Elsevier, 199-259.

[27] Padoan R, Steemers T, Klein M, Aalderink B, de Bruin G: Quantitative hyperspectral imaging of historic documents. 9th International Conference on NDT of Art. 2008, Jerusalem, Israel

[28] Frentress, Z.; Young, L.C.; Edwards, H.D. Field Photometer with Nine-Element Filter Wheel. Appl. Opt. 1964, 3, 303–308.

[29] Wyatt CL. Infrared spectrometer: Liquid-helium-cooled rocketborne circular-variable filter. Appl Opt 1975;14:3086–3091

[30] Sequential Filter Wheel Multispectral Imaging Systems Eichenholz, Jason M. 2010 Applied Industrial Optics: Spectroscopy, Imaging and Metrology, Paper# ATuB2

[31] Comparison of Acousto-optic and Liquid Crystal Tunable Filters for Laser-Induced Breakdown Spectroscopy Dimitra N. Stratis, Kristine L. Eland, J. Chance Carter, Samuel J. Tomlinson, and S. Michael Angel Applied Spectroscopy Vol. 55, Issue 8, pp. 999-1004 (2001)

[32] Imaging Spectrometers for Fluorescence and Raman Microscopy: Acousto-Optic and Liquid Crystal Tunable Filters Hannah R. Morris, Clifford C. Hoyt, and Patrick J. Treado Applied Spectroscopy Vol. 48, Issue 7, pp. 857-866 (1994)

[33] Miller PJ. Use of tunable liquid crystal filters to link radiometric and photometric standards. Metrologia 1991;28:145–149.

[34] Liquid Crystal Tunable Filter Raman Chemical Imaging Hannah R. Morris, Clifford C. Hoyt, Peter Miller, and Patrick J. Treado Applied Spectroscopy Vol. 50, Issue 6, pp. 805-811 (1996)

[35] Shonat R, Wachman E, Niu W, Koretsky A, Farkas D. Near-simultaneous hemoglobin saturation and oxygen tension maps in mouse brain using an AOTF microscope. Biophys J 1997;73:1223–1231.

[36] Igor B Kutuza, Vitold Ed Pozhar, Vladislav Iv Pustovoit, "AOTF-based imaging spectrometers for research of small-size biological objects," Proc. SPIE 5143, Novel Optical Instrumentation for Biomedical Applications, (14 October 2003);

[37] Polarization Selective Wavelength Tunable Filter Jeroen Beeckman , Tian Hui , Pieter J. M. Vanbrabant , Robert Zmijan & Kristiaan Neyts Pages 19-28 | Published online: 01 Jun 2009

[38] Single sensor that outputs narrowband multispectral images Linghua Kong,a,* Dingrong Yi,a Stephen Sprigle,a Fengtao Wang,b Chao Wang,b Fuhan Liu,b Ali Adibi,band Rao TummalabaGeorgia Institute of Technology accepted for publication Nov. 9, 2009; published online Jan. 7, 2010.

[39] Lapray, Pierre-Jean & Wang, Xingbo & Thomas, Jean-Baptiste & Gouton, Pierre. (2014). Multispectral Filter Arrays: Recent Advances and Practical Implementation. Sensors (Basel, Switzerland). 14. 21626-59. 10.3390/s141121626.

[40] Mejia-Melgarejo, Yuri & Patricia Villarreal-Dulcey, Ofelia & Arguello, Henry. (2015). Adjustable spatial resolution of compressive spectral images sensed by multispectral filter array-based sensors. Revista Facultad de Ingeniería Universidad de Antioquia. 2016. . 10.17533/udea.redin.n78a12.

[41] Ramanath, R.; Snyder, W.E.; Qi, H. Mosaic multispectral focal plane array cameras. Infrared Technology and Applications. Proc. SPIE 2004, 5406, 701–712

[42] Miao, L.; Qi, H. The design and evaluation of a generic method for generating mosaicked multispectral filter arrays. IEEE Trans. Image Process. 2006, 15, 2780–2791.

[43] Zimmermann T. () Spectral Imaging and Linear Unmixing in Light Microscopy. In: Rietdorf J. (eds) Microscopy Techniques. Advances in Biochemical Engineering, vol 95. Springer, Berlin, Heidelberg

[44] A. V. Kanaev, M. R. Kutteruf, M. K. Yetzbacher, M. J. Deprenger, and K. M. Novak, "Imaging with multi-spectral mosaic-array cameras," Appl. Opt. 54, F149-F157 (2015)

[45] Romuald Jolivot, Pierre Vabres, Franck Marzani. Reconstruction of hyperspectral cutaneous data from an artificial neural network-based multispectral imaging system. Computerized Medical Imaging and Graphics, Elsevier, 2011, 35, pp.85-88.

[46] Shen-En Qian, "Hyperspectral data compression using a fast vector quantization algorithm," in IEEE Transactions on Geoscience and Remote Sensing, vol. 42, no. 8, pp. 1791-1798, Aug. 2004

[47] A. Karami, M. Yazdi and G. Mercier, "Compression of Hyperspectral Images Using Discerete Wavelet Transform and Tucker Decomposition," in IEEE Journal of Selected Topics in Applied Earth Observations and Remote Sensing, vol. 5, no. 2, pp. 444-450, April 2012.

[48] https://www.arduino.cc/en/Reference/Stepper

[49] http://astronomy-imaging-camera.com/software/

[50] https://github.com/stevemarple/python-zwoasi

[51] https://matplotlib.org/

[52] https://github.com/python/cpython/blob/2.7/Lib/threading.py

[53] https://github.com/skvark/opencv-python